1982

Flume experiments on bedforms and structures at the dune-plane bed transition

Francis P.J. Lockett
Wilfrid Laurier University

CANADIAN THESES ON MICROFICHE

I.S.B.N.

THESES CANADIENNES SUR MICROFICHE

National Library of Canada
Collections Development Branch

Canadian Theses on
Microfiche Service

Ottawa, Canada
K1A 0N4

Bibliothèque nationale du Canada
Direction du développement des collections

Service des thèses canadiennes
sur microfiche

NOTICE

The quality of this microfiche is heavily dependent upon the quality of the original thesis submitted for microfilming. Every effort has been made to ensure the highest quality of reproduction possible.

If pages are missing, contact the university which granted the degree.

Some pages may have indistinct print especially if the original pages were typed with a poor typewriter ribbon or if the university sent us a poor photocopy.

Previously copyrighted materials (journal articles, published tests, etc.) are not filmed.

Reproduction in full or in part of this film is governed by the Canadian Copyright Act, R.S.C. 1970, c. C-30. Please read the authorization forms which accompany this thesis.

THIS DISSERTATION
HAS BEEN MICROFILMED
EXACTLY AS RECEIVED

AVIS

La qualité de cette microfiche dépend grandeme
la qualité de la thèse soumise au microfilmage.
avons tout fait pour assurer une qualité supé
de reproduction.

S'il manque des pages, veuillez commu
avec l'université qui a conféré le grade.

La qualité d'impression de certaines page
laisser à désirer, surtout si les pages originales o
dactylographiées à l'aide d'un ruban usé ou si l'u
sité nous a fait parvenir une photocopie de ma
qualité.

Les documents qui font déjà l'objet d'un
d'auteur (articles de revue, examens publiés, et
sont pas microfilmés.

La reproduction, même partielle, de ce mic
est soumise à la Loi canadienne sur le droit d'a
SRC 1970, c. C-30. Veuillez prendre connaissan
formules d'autorisation qui accompagnent cette th

LA THÈSE A ÉTÉ
MICROFILMÉE TELLE QUE
NOUS L'AVONS REÇUE

FLUME EXPERIMENTS ON BEDFORMS AND STRUCTURES AT THE DUNE-PLANE BED TRANSITION

by

Francis P.J. Lockett

Submitted to fulfill the requirements of
Geography 699

FLUME EXPERIMENTS ON BEDFORMS AND STRUCTURES AT THE DUNE-PLANE BED TRANSITION

by

Francis P.J. Lockett

WILFRID LAURIER UNIVERSITY

WATERLOO

1982

ACKNOWLEDGEMENTS

Initially, I wish to thank Dr. B.G. Craig and Dr. T.J. Day for permission to use the flume facility at the Terrain Sciences Division, Geological Survey of Canada. Thanks are also expressed to the Natural Sciences and Engineering Research Council of Canada for their financial assistance provided through Dr. Houston Saunderson. I would like to thank the members of my thesis committee Dr. Kenneth Hewitt, Dr. Gunars Subins, the chairman Dr. Robert McCauley and my outside examiner Dr. David Lawson. Thanks are also expressed to Miss Julie Stanfel and Mr. James Lockett for their timeless support. Finally and most importantly, I wish to thank my thesis advisor Dr. Houston C. Saunderson who made it possible for the research to be conducted and whose guidance and enthusiasm over the last two years were invaluable.

TABLE OF CONTENTS

LIST OF FIGURES

LIST OF TABLES

ABSTRACT

A tiltable, recirculating flume, 18 metres long and 76 cm. wide was used to investigate bedforms and structures near the transition between dunes and a plane bed for a moderately sorted, coarse sand. At Froude numbers ranging from about 0.4 to 1.0, three dune types developed: (1) asymmetrical (triangular) dunes, (2) convex (symmetrical) dunes and (3) humpback (whaleback) dunes. Asymmetrical dunes had gentle, long stoss sides and steep, short lee sides and contained cross-stratification with a maximum dip mostly about 30° to 35°. Flow separation and avalanching were strongly developed to the lee of these dunes. Convex dunes formed when the bed was thin and had longitudinal profiles that were convex-upward with stoss and lee sides of equal steepness. Internal cross-beds were likewise convex and formed from draping of sediment over the lee sides rather than from avalanching. Humpback dunes were the most distinctive bedforms in that on each dune profile the point of maximum elevation was offset from the top of the foreset (avalanche) slope. Immediately downstream from this maximum point, low-angle topset bedding merged uninterruptedly into steep foreset beds and these into bottomsets, producing sigmoidal bedding inside each dune. Although foreset slopes were much shorter in humpback dunes than in asymmetrical, their steepness remained mostly about 30° to 35° right up to the change to a plane bed at a Froude

number of about 1.1. For one other run a plane bed also formed but at a Froude number of about 1.7, a rather high value for a plane bed just beyond the dune bed phase. This second plane bed may be that which occurs at Froude numbers larger than those for in-phase waves.

GLOSSARY

Aggradation rate - The speed at which any bed configuration thickens vertically or protrudes into flow.

Bed load - Sediment that is transported by rolling, sliding or creeping along the bed surface.

Bed material load - That part of the sediment load which consists of both bed load and saltating load.

Froude number - A measure of tranquility of flow, defined as $\bar{u}/\sqrt{g\bar{d}}$ in which $\bar{u}$ = fluid mean velocity, g = acceleration due to gravity and $\bar{d}$ = mean fluid depth where $Fr > 1$ is considered to be supercritical flow and $Fr < 1$ is considered to be subcritical flow.

Lower flow regime - Flow in sand channels which generates bed configurations in the order of ripples, ripples on dunes and dunes. All bedforms are out of phase with the water surface.

Progradation rate - The speed at which any bed configuration migrates downstream.

Reynolds number - A measure of turbulence in the flow, defined as $R = \bar{u}\bar{d}/\upsilon$ in which $\bar{u}$ = fluid mean velocity, $\bar{d}$ = mean fluid depth and υ = kinematic viscosity of fluid where $R \leq 500$ is considered laminar flow and $R \geq 2000$ is considered turbulent flow. A transition may occur between 500 and 2000 where, if the boundary between the bed and the laminar sub layer is rough, turbulent flow conditions may occur as low as 500. However, if the boundary is smooth, laminar flow may persist up to 2000.

Rheological fronts - These are very low (< 1 cm) sand fronts which migrate downstream as ballistic dispersions as interparticle collision becomes prominant in flow near the bed.

Saltating load - Sediment that is transported by bouncing along the bed surface.

Transitional bedforms - Bed configurations generated at the transition between lower flow regime dunes and upper flow regime plane beds.

Upper flow regime - Flow in sand channels which generates bed configurations in the order of plane beds, antidunes and chutes-and-pools. All bedforms are in-phase with the water surface.

Velocity profile - Horizontal components of flow velocity in relation to depth at a vertical section over a point on the bed.

1

INTRODUCTION

Many significant aspects of fluvial hydraulics, bedform mechanics and the internal structure of bedforms in alluvial channels have been thoroughly investigated both in the field and the laboratory over the past century. In most cases, important questions have been answered and there now exists an adequate understanding of the genesis of sedimentary structures generated by flow in open channels. With a grasp of the broad scope of the field and the magnitude of the interrelated nature of the variables involved, it should be possible with continuing research and collection of sedimentological data to formulate a more composite picture superior to any obtained thus far.

Early research involving the development of sedimentary bed configurations by current action in open channels was conducted, amongst others, by Sorby (1859). In a qualitative manner, using invented words and contrived similes, he developed general arguments dealing with the genesis of small scale ripples or "drift-bedding".

One of the most thorough and complete groups of experimental data ever collected resulted from a series of classical flume experiments conducted by Gilbert (1914). The experiments were sponsored jointly by the U.S. Geological Survey and the University of California.

Gilbert's intentions were to investigate the natural laws controlling the movement of sediment along river channels. In all,

more than one thousand experiments were completed using bed material consisting of natural sands and gravels. He concluded that an alluvial boundary in a river channel was formed of cohesive or non-cohesive materials that had been or could be transported by flow. At some discharges, the sediment forming the alluvial boundary would not move and the river channel would essentially be a rigid one. However, once general movement of the bed material commenced, the boundary could then be moulded into many geometric forms. Continuing investigations of the genesis of sedimentary structures generated by flow in alluvial channels slowly yielded valuable information concerning fluvial hydrodynamics and sediment transport.

The idea most clearly developed by Simons and co-workers (Simons, Richardson and Albertson, 1961; Simons and Richardson, 1962, 1963, 1966; Simons, Richardson and Nordin, 1965; Guy, Simons and Richardson, 1966), that a loose sediment bed beneath turbulent flows assumes a definite sequence of bed configurations as flow strength or tractive force is increased, has found wide application in sedimentology. In their various papers, the authors demonstrate that sedimentary bed configurations may be broadly classified by their shape and spacing, their resistance to flow, by their phase relationship to water surface and by their mode of sediment transport. By using such criteria, two flow regimes were recognized; the "Lower Flow Regime" and the "Upper Flow Regime", with a "Transition" between the two. These subdivisions of flow regimes were considered by the authors to be quite general but were a means of conveniently grouping different bed configurations.

In the lower flow regime at constant depth but increasing

velocity, a sequence of bed configurations were observed to follow the order: no movement, ripples, ripples superimposed on dunes, and dunes. The water surface was observed to be out of phase with the bed surface and there existed a relatively large separation zone downstream from the crest of ripples and dunes where backflow tended to steepen and reinforce the angular shape of these structures. The most common mode of sediment transport was observed to be bedload, and deposition and storage of the sediment was through avalanching action on the foreset slopes of these structures. Flow was tranquil or subcritical as measured by the Froude number ($Fr < 1$) where:

$$Fr = \bar{u}/\sqrt{gd}$$

in which: $\bar{u}$ - average velocity
g - acceleration of gravity
$\bar{d}$ - average depth of flow

In the upper flow regime at constant depth but increasing velocity, a sequence of bed configurations were observed to follow the order: plane bed, antidunes with standing waves, antidunes with breaking waves and chutes-and-pools. The water surface was observed to be in-phase with the bed surface except when antidunes broke, and normally no flow separation was observed between the water and the boundary of the sedimentary structures. The most common mode of sediment transport observed was sheet and suspended load transport. Flow was observed to be supercritical ($Fr > 1$).

The transition between the lower and upper flow regimes was observed to be variable, depending largely on antecedent conditions. The dune bedform from the lower flow regime was observed to continually exist even as variables such as depth and slope were increased to values more consistent with a plane bed of the upper flow

regime although it did decrease in amplitude and wavelength. Conversely, a plane bed from the upper flow regime was observed to continually exist as depth and slope were decreased to values more consistent with dunes of the lower flow regime.

It was also noted by the authors that the primary variables determining what particular bed configuration would be generated at a specific flow velocity were the fall velocity of the bed material and the flow depth.

Southard (1971) demonstrated from dimensional analysis that relationships exist between bed configurations and dimensionless combinations of flow and sediment variables. Using experimental data from a variety of sources, he designed diagrams for presenting the sequence or phases of bed configurations based on variables involving fluid, sediment and flow. This graphical approach is not a unique one and has been attempted amongst others by Simons and Richardson (1963) and Allen (1968a). They met with limited success since their diagrams involved using bed shear stress as a coordinate and it is itself a function of bed configuration in such a way that in some cases more than one bed configuration may correspond to a single value of bed shear stress. Southard suggested that bed state was governed by seven variables and that given a set of these variables implies a unique bed state: d - depth of flow; $\bar{U}$ - mean velocity of flow; p - density of fluid; υ - viscosity of fluid; $\bar{D}$ - mean size of sediment; p_s - density of sediment; g - acceleration due to gravity. This approach provides a more concrete picture of the relationship among bed configurations since each point from experimental flume data corresponds on his boundary diagrams to one and only one bed state.

From inspection of Southard's boundary diagrams it is evident that there exists a deficiency in information to explain such basic phenomena as transitional bedforms. Ripples and their cross-laminae, dunes and their cross-stratification, plane beds and parallel laminae, antidunes and backset laminae are now all well documented bedforms and structures for both experimental and field investigations, but reports on the transitional bedforms between these well known types are less abundant. The transition from ripples to lower flat (plane) bed has been investigated for coarse sand (Southard and Boguchwal, 1973) and from ripples to dunes (Banks and Collinson, 1975) for medium sand. Mathematical, conceptual treatment of the dune to plane bed transition has been done by Engelund and Fredsøe (1974) who tested their model against the experimental data of Guy, Simons and Richardson (1966). Jopling and Forbes (1979) made some experimental observations on the ripple to upper plane bed transition in coarse silt. Allen and Leeder (1980) analyzed stability criteria for the transition from an upper plane bed to dunes and ripples for decelerating flows. Still deficient though are detailed observations of bedform shape and associated stratification in flumes and natural streams for the dune to plane bed transition.

The objectives of the author in this report are to investigate and interpret from laboratory flume experiments what particular bedforms and bedding structures are generated at the transition from lower flow regime dunes to upper flow regime plane beds. The experimental approach shown by Gilbert and Simons et. al. to be so successful in analyzing form and structural relationships to flow was chosen over that of field investigations since the laboratory offered

more control over important parameters such as velocity and depth. In natural channels, nonuniform velocity and depth result in multiple bedforms across a section whereas in the laboratory, with close to equilibrium flow conditions, the same bedform could be established throughout the length of the flume. In recent literature, velocity and depth have been shown to correlate strongly with bedform dimensions. By varying these parameters, it is possible to generate transitional bedforms from which specific measurements on dimension and stratification may be made and hydraulic data can be cautiously extrapolated.

2

EXPERIMENTAL APPARATUS

Description of the Flume

The experiments conducted to investigate bedforms and associated structures in the transition between dune and plane beds were performed using the Sedimentation Flume housed in the Terrain Sciences Division of the Geological Survey of Canada, Ottawa, Ontario (Fig. 1).

The main channel of the flume is 18.3 m. long, 76 cm. wide and 60 cm. deep (Fig. 2 and 3). The flume is tiltable and is capable of recirculating sediment up to 4 mm. in diameter. "The entire apparatus is set above the laboratory floor level with a stationary working platform along the entire length on both sides of the channel. Rigidity is provided by two steel longitudinal supporting I-beams situated below the main channel. The entire channel is supported at three equally spaced points. The downstream support is the pivot on which the channel tilts. The center and upstream supports are provided by electric jacks. The jacks are synchronized and are capable of tilting the main channel to a maximum slope of 0.05 or 90 cm. vertically at the upstream end." (McDonald, 1972, pp. 3-4)

The viewing sections of the flume's channel walls are half-inch plate glass in individual panels 1.8 m. long. Ten of these sections on either side of the channel, separated by steel support beams, allow for observation of deposition at the head of the channel through

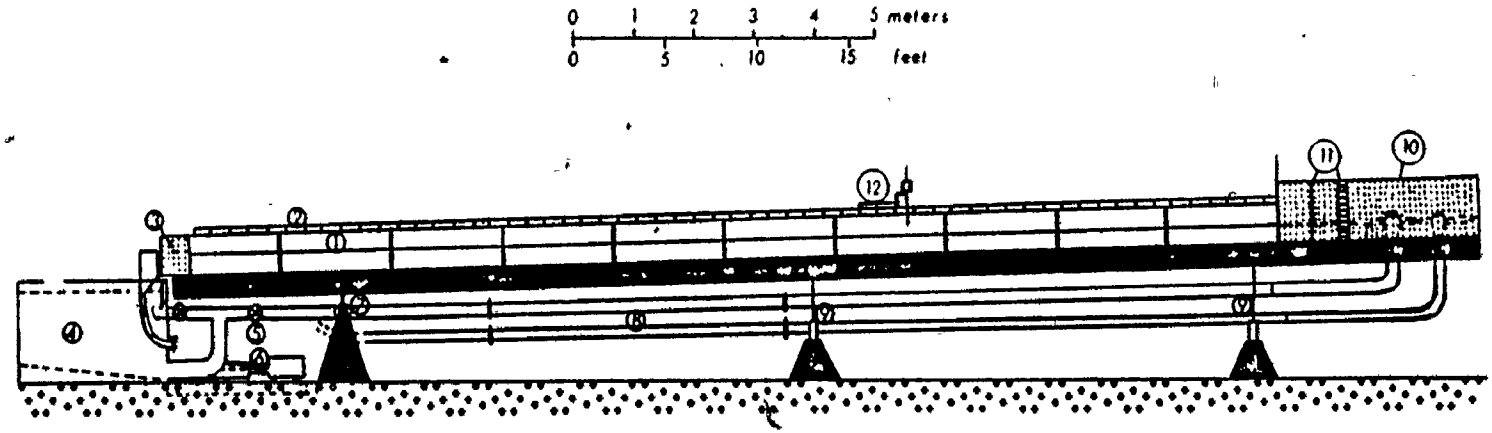

1. main channel
2. rails
3. tailgate assembly
4. tail tanks
5. flow-control valves
6. pump and motor
7. pivot support
8. transportation section of return pipe
9. jack supports
10. headbox
11. baffles
12. instrument carriage

FIG. 1

Generalized longitudinal diagram of flume (after B.C. McDonald 1972).

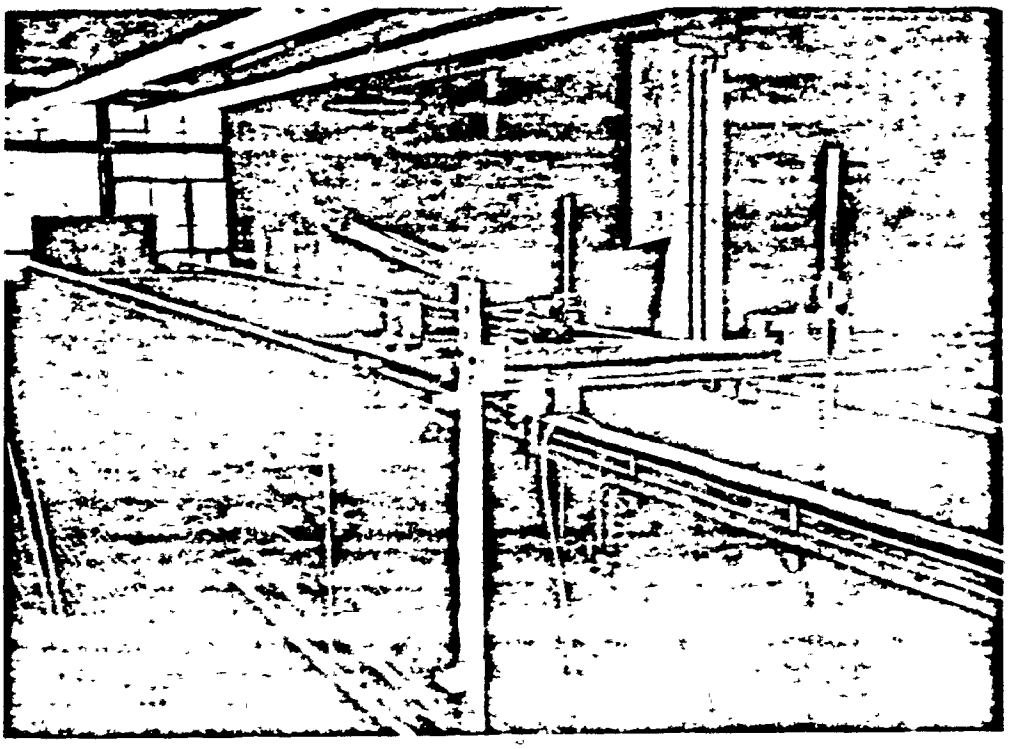

FIG. 2

Longitudinual view of main channel, looking downstream from the 9 meter mark.

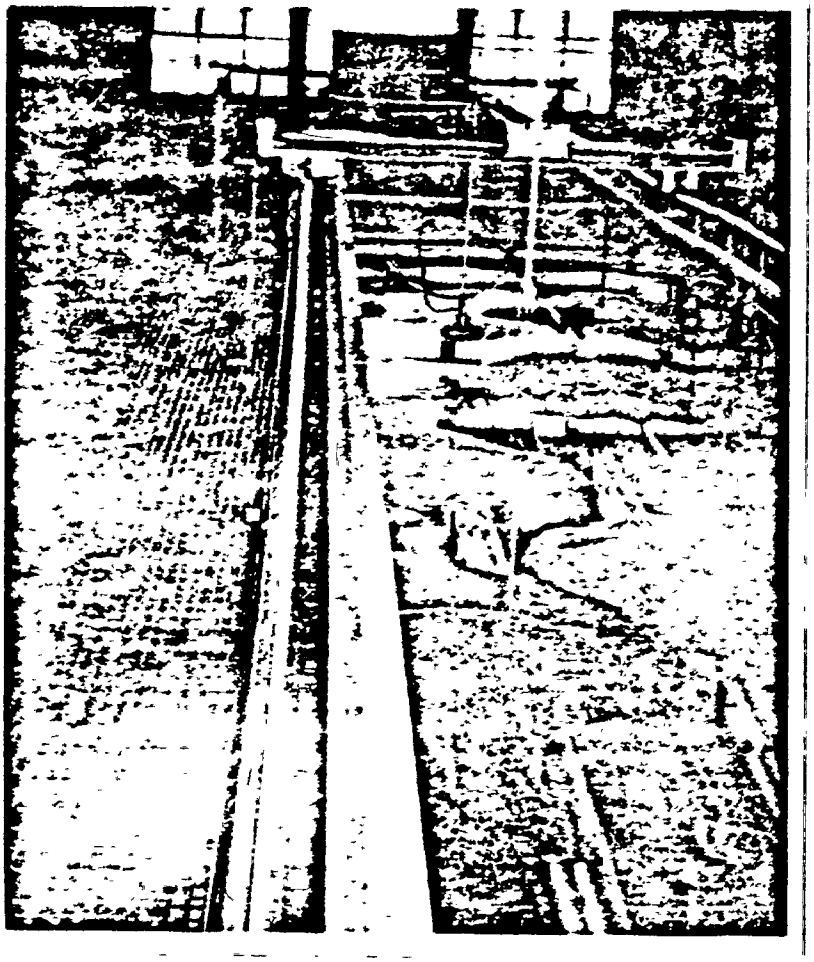

FIG. 3

Plan view of main channel, looking downstream from the 5 meter mark.

changing bed morphology and mechanics over its length, to the ultimate erosion of the bed at the downstream end.

Over the entire length of the channel walls, stainless steel rails are mounted which support and guide a three wheeled instrument carriage. It is possible to move the carriage along the flume to any spot from which measurements can be taken along or across the channel (Fig. 2 and 3).

At the upstream end of the channel, a plate aluminum headbox 3 m. in length, 76 cm. wide and 96 cm. deep introduces flow through a T-fitting and a series of straightening baffles into the main channel. The T-fitting on the floor of the headbox directs the flow downward from which point the flow is directed downstream through two baffles. "One baffle constrains the streamlines for a straight distance of 15 cm. through 4 cm. square tubular openings in an attempt to minimize artificial turbulence. A second baffle consists of a nest of horizontal rods oriented across the channel and spaced so as to preferentially retard the basal part of the flow in an attempt to aid in the development of a stable vertical velocity profile. The flow then passes beneath an overshot headgate into the main channel." (McDonald, 1972, p.7). At the downstream end of the channel another overshot sealing tailgate is used to adjust the water depth or stop the flow, filling the flume and providing a low energy environment conducive to bedform preservation and bed sampling.

Once past the overshot tailgate, the flow free-falls into a reservoir system. This reservoir measures 6.7 m. long, 2.4 m. wide and 1.5 m. deep with a holding capacity of 23.8 $m.^3$ of water and sediment. Of the three holding tanks in this system, the central one acts as the

"active" reservoir, receiving discharge from the channel and from which point sediment and water are pumped back to the headbox. The floor of this reservoir slopes toward the pump intake in order to minimize storage of sand in the tank. On either side of this active reservoir are found "passive" reservoirs. The floor of both reservoirs are flat in order to maximize water storage capacity. The partitions separating the two passive reservoirs from the active reservoir are 15 cm. below the encompassing outer wall, thus allowing the full capacity of the reservoir to be used as storage which is sufficient enough to hold all of the water in the system when the flume is not in operation.

"Water and sediment are pumped from the active reservoir back to the headbox by an electric, constant-speed, direct-drive, axial-flow, open-impeller pump." (McDonald, 1972, p.5). The inside diameter of the steel return pipe measures 25 cm.

The proportion of discharge that is directed to the headbox is controlled by a valve system and a bypass line which directs discharge back to the active reservoir. The valve system enables the operator to control flow discharge for any given experiment.

The bypass valve has a twofold purpose. Its primary function is to allow the operator to vary flow discharges during any given experiment. Its secondary function is to keep the water and sediment mixture churned up and moving in the active reservoir, thereby minimizing sedimentation on the floor of this reservoir.

In the straight section of the return pipe, a 5 m. length of smooth, transparent acrylic pipe is mounted with the same inside diameter as the rest of the pipe system. The transparent section permits examination of the sediment transport processes and resulting

bed forms in pipe flow. In addition, the transparency allows for a visual check of sediment storage in the return pipe (see McDonald, 1972 for more complete information on the apparatus).

Sediment Handling

The storage of sediment in the laboratory is provided by a number of raised wooden bins with forward sloping floors. Each bin has a capacity of 4.5 tons of sediment. A sliding gate at the bottom of each bin allows the operator to withdraw any desired amount of sediment. The sediment is then screened to ensure that the large sized fractions greater than 4 mm. are removed. A series of two conveyor belts transport the sediment directly to the active reservoir where it enters the flow system of the flume. Feed rate is manually controlled by the conveyor operator.

Transfer of the sediment from the flume back to the bins or to a convenient area for disposal is accomplished by two steps. The first step involves diverting the sediment discharge to one of the passive reservoirs by means of a turning elbow. This elbow is attached to the tailgate assembly of the channel and is suspended over the active reservoir, diverting the flow directly to the passive reservoir. By maintaining high flow discharge and low flow depth in the channel, net deposition occurs in the passive reservoir. Water is then returned to the system when it overflows the retaining wall separating the two reservoirs. By diverting flow in this fashion, approximately 95 percent of the sediment in the system is deposited in the passive reservoir during one hour of operation. The remaining 5 percent of the sediment which is fine in nature (silts and clays), are kept in suspension and continue to move throughout the system.

The second step involves the increasing of flow depth in the channel while maintaining a constant flow discharge, thereby decreasing velocity. Thus, the remaining 5 percent of the sediment settles out in this low energy environment and is mostly deposited on the main channel floor. By shovelling the sediment from the passive reservoir and the main channel onto the conveyor belts, the sediment may be returned to storage or disposed.

Measurement of Hydraulic Parameters

Surface velocity - Surface velocities were measured by timing the travel of a surface float (ping-pong ball) over a known distance. The 300 cm. section of the channel from the 7.5 m. to 10.5 m. mark on the flume was selected to be the distance the float would travel, being about halfway along the channel and thus least influenced by surface turbulence from entrance and exit effects. The float was placed centre-channel approximately 1 m. upstream of the 7.5 m. mark (to allow the float to accelerate to surface velocity) and was timed by a stopwatch as it travelled past the 7.5 m. mark over the 300 cm. distance. At lower flow velocities in the experiments when water surface undulations were slight, the beam from a neon-hydrogen laser focused at a right angle to flow at the 10.5 m. mark was used to indicate, when visually broken, the precise time it took for the surface float to travel 3 m. If the surface float strayed more than an arbitrary 5 cm. from centre-channel over the 300 cm., the time results were invalidated and the procedure repeated due to possible frictional drag created by the sidewalls of the channel. This procedure was duplicated five times for each run and an average surface velocity was calculated for each. Mean velocities were approximated for each run as 0.8 times the surface

velocity, following the practice of Fahnestock (1963, p. A30) and Williams (1967, p. B5) for shallow flows.

Velocity profiles and water depth - Velocity profiles were obtained by measuring point velocities with a calibrated pitot tube using two water-air manometers. The difference between the two levels of water in the manometers is a hydraulic head measurement which is a measurement of the potential energy at that point in flow. This measurement was converted to a point velocity by solving for "υ" in the following equation:

$$m\ g\ h = 1/2\ m\ \upsilon^2$$

in which: $m\ g\ h$ - potential energy of flow

$1/2\ m\ \upsilon^2$ - kinetic energy of flow

where: m = mass

g = acceleration due to gravity or $g = 9.81$ m./sec.^{2}

h = difference in manometer levels

υ = point velocity

The pitot tube was calibrated against surface and middle vertical flow velocities obtained through the use of a Gurley current meter. This current meter, however, was considered too bulky and not sensitive enough for near bottom and trough measurement to be exclusively used for determining point velocities. The general accuracy of the pitot tube was then tested by comparing a calculated mean channel velocity from vertical point velocities against a mean velocity calculated from surface velocities, determined through the use of surface floats.

The pitot tube was attached to the point gauge and mounted vertically to the instrument carriage and was capable of being moved

vertically or horizontally across the flume, thus allowing for the measurement of point velocities anywhere in the flow. A stainless steel foot was also attached with the pitot tube to the point gauge. This foot allowed the operator, especially in flows with abundant suspended sediment, to determine where the bed was situated. Without this foot the pitot tube could be unknowingly lowered into the bed indicating an incorrect bed depth and little if any flow velocity. This foot was also used in determining where the water surface was with respect to the bed. Due to the undulating characteristics of the water surface at higher flow velocities, the point at which the foot was 50% of the time in and 50% of the time out of the water was interpreted as being the surface.

Velocity profiles were constructed from pitot tube measurements of point velocities from the bed upward to the surface of flow for all the runs. Velocity profile data was determined as rapidly as the pitot tube could stabilize.

In order to allow for bedform migration in runs with higher velocities, the pitot tube was moved during the course of taking the profile. This was executed in order to keep the tube at the same location with respect to the structural profile. If the pitot tube was not moved during data collection, a vertical profile for a location such as a dune trough might have some upper point velocities indicating a dune crest, if the crest of a dune migrated to where the trough had been before the measurements had been completed.

For eleven of the twelve runs conducted, point velocities were recorded at 5 cm. intervals starting at the bed and moving to the water surface. In Run #12, point velocities were recorded in 1 cm.

intervals due to a shallow flow. All velocity profiles were recorded midstream, 38 cm. from the channel walls, in an attempt to minimize possible frictional drag on the flow by the sidewalls. Water depth for each run was then established from velocity profile data.

Water temperature was measured with a mercury thermometer to the nearest 1.0°C. Temperature measurements were only made after quasi-equilibrium conditions were met. Temperatures recorded were the average of two temperature measurements taken at the beginning and the end of the data collection phase of each run.

Measurements of bedform dimensions - Bedform dimensions were measured through the viewing sections of the channel walls using conventional measuring devices. The bed-surface observations were made either through the viewing sections if the water was sufficiently clear or from the flume at the end of the run after the water had been carefully drained out. Dimensions such as height, wavelength, steepness of stoss and lee sides were measured visually and in some cases, recorded photographically for the different structures. Observations and measurements were also recorded for stratification, degree of sorting, thickness of laminae and number of laminae deposited per unit of time. Between runs, the bed was flattened artificially.

3

EXPERIMENTAL PROCEDURE

Hydraulic Conditions of the Flow

The experiments were conducted in the flume housed in the Terrain Sciences Division of the Geological Survey of Canada from July 18 to August 12, 1980. In all, twelve experimental flume runs were conducted with varying hydraulic conditions in each. Moderately sorted, medium to coarse sand was used in the experiments (Fig. 4, Appendix A) and was introduced from the storage bins to the central end tank using conveyor belts and then pumped via the return pipe to the headbox and into the channel. Although the flume is equipped with two pumps, only the 30 cm. pump was used to generate flows. Fluid depth and discharge were controlled by opening and closing a valve operating a bypass from the return pipe back to the end tank and by adjusting the overshot tailgate. The water-sediment mixture was recirculated for five to six hours during each run before any measurements were made to ensure the development of a related family of bedforms along most of the flume length (barring approximately one metre on either end due to possible entrance and exit effects). By recirculating the water-sediment mixture in such a manner, conditions were simulated of a long reach of river channel. By developing a related family of bedforms or particular types of bed configurations along the length of the flume, equilibrium flow (Simons, Richardson and Nordin, 1965) conditions

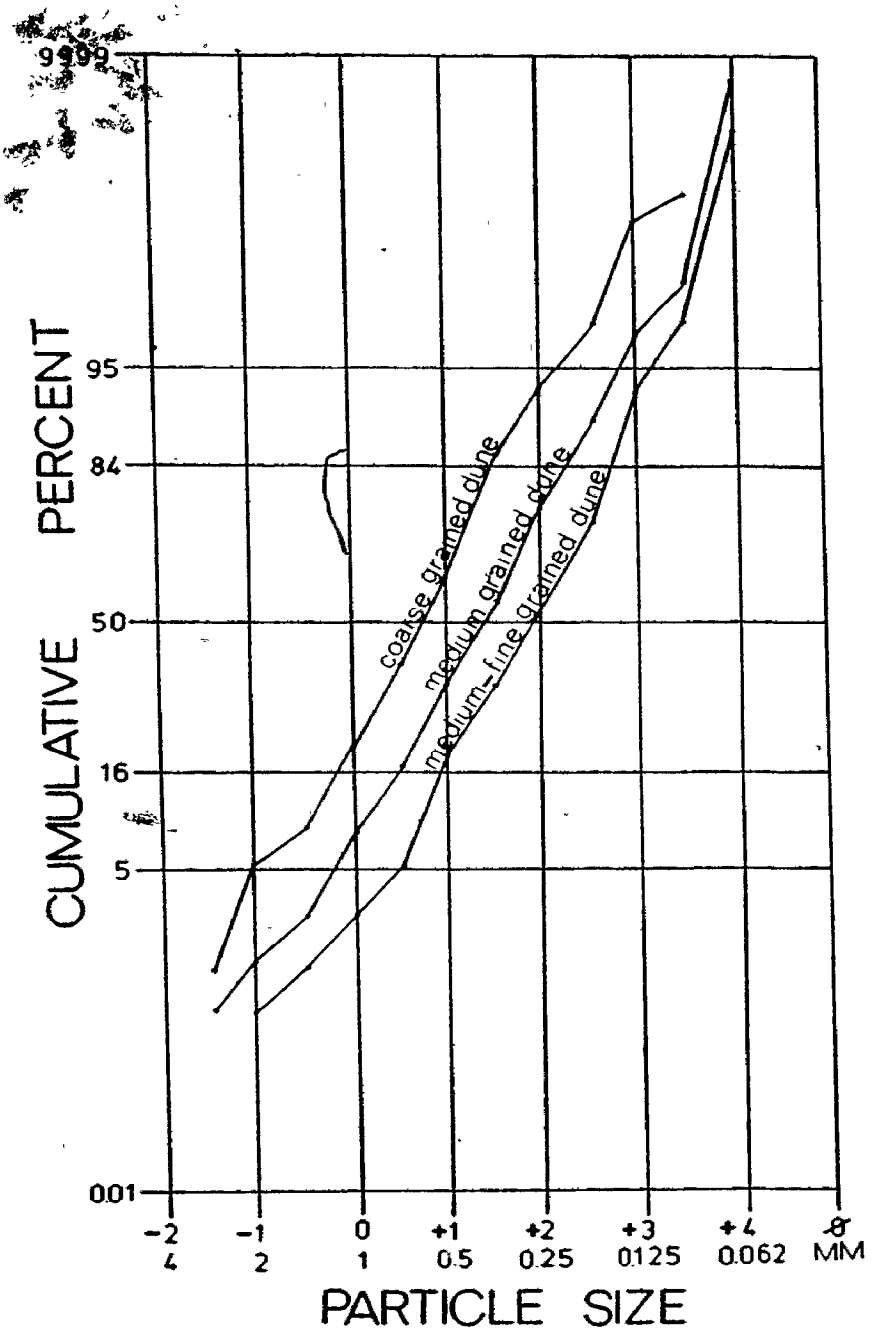

FIG. 4

Cumulative frequency size distributions for sediments used in the experiments. Channel samples were taken of the dunes at centre channel, 5 cm. upstream from the crest of the foreset slope. Although the sediment was mixed thoroughly before being introduced to the return pipe and flume channel, sorting of sizes into coarse, medium and medium to fine grained dunes occurred along the channel. The coarse-grained dune was sampled from experimental Run #8 and the medium and medium to fine grained dunes from Run #4. The median diameter for all three dunes is about +1.50 with approximately 50% of the combined distribution containing medium to coarse sand, coarse sand, very coarse sand and granule gravel.

were approached. However, quasi-equilibrium rather than true equilibrium flows were most probably established due to a certain unsteadiness in the flow related to short circulation times (5 to 6 hours). Equilibrium flow however, should not be confused with steady, uniform flow since velocity may vary at a point and from point to point over different bed configurations. Steady, uniform flow does not exist in a mobile-boundary alluvial channel unless the bed is plane with no sedimentary structures protruding into the flow.

The main objective of the author was to delimit the range of hydraulic conditions over which dunes became transformed or "washed-out" (Simons, Richardson and Nordin, 1965; Simons and Richardson, 1966; among others). As is true for most other flumes, the prime limitation of the experiments was the small range of attainable flow depths which were never greater than 45 cm. and were mostly between 20 and 40 cm. Table 1 is a summary of the hydraulic conditions that existed during the experiments.

Hydraulic radius ($R = A/P$ where A is equal to the cross-sectional area or width times depth, and P is equal to the wetted perimeter or width plus twice the depth) decreased generally from the first to last run as a consequence of slight decreases in water depth. This decrease, combined with a general increase in mean velocities from 52 cm./sec. in Run #1 to 160 cm./sec. in Run #12 resulted in a corresponding increase in Froude number from 0.38 to 1.75.

Changes in Reynolds number ($Re = \bar{U}\bar{d}/\upsilon$, where $\bar{U}$ is average velocity, $\bar{d}$ is average depth and υ is kinematic viscosity) resulted from velocity changes rather than temperature which only ranged from 23°C. to 25°C. The magnitude of these changes was not considered to be

Table 1: Summary of Experimental Measurements and Hydraulic Calculations*

RUN	SURFACE VELOCITY (cm/sec)	MEAN VELOCITY (cm/sec)	HYDRAULIC RADIUS(R) (cm)	TEMP. (°C)	KINEMATIC VISCOSITY (stokes)	REYNOLDS NUMBER (Re)	BEDFORM	FROUDE NUMBER (Fr)
1	65.6	52.48	19.34	23	0.009325	108,843	h./a.	0.38
2	64.3	51.44	18.58	24	0.009111	104,901	h./a.	0.38
3	79.2	63.36	18.84	24	0.009111	131,017	h./a.	0.47
4	85.7	68.56	17.93	24	0.009111	134,922	h./a.	0.52
5	100.0	80.00	16.59	24	0.009111	145,670	h./a.	0.63
6	93.8	75.04	17.42	24	0.009111	143,474	h./a.	0.57
7	121.0	96.80	15.19	24	0.009111	161,386	h./a.	0.79
8	130.4	104.32	15.25	24	0.009111	174,610	h./a.	0.85
9	142.9	115.32	15.64	24	0.009111	197,959	h./a.	0.93
10	150.0	120.00	14.48	25	0.008904	195,148	h.	1.01
11	157.9	127.32	14.25	25	0.008904	203,763	h./p.	1.08
12	200.0	160.00	8.53	24	0.009111	149,796	p.	1.75

*No physical significance is attached to the decimal places in velocity calculations. They have been maintained just to reduce rounding errors in the calculation of the Froude number. Hydraulic radius was substituted for depth in calculating Froude number.

a. = asymmetrical dune

h. = humpback dune

p. = plane (flat) bed

of physical significance as an important variable when explaining variations in bedforms since a modal grouping of Reynolds numbers was present which does not show a close correlation to progressive changes in bedform characteristics. The Reynolds number was therefore rounded off to the nearest order of magnitude which for all runs was 1.0×10^5. Subtle changes in bedform characteristics and stratification were considered related more to variations in Froude number where progressive increases in Froude number correlated closely to changes in bedform characteristics.

Dune Profiles Generated In Flow

During the course of the experiments, three distinct shapes of dunes formed and were designated (a) asymmetrical dunes, (b) convex, symmetrical dunes, and (c) humpback dunes (Fig. 5) (convex, symmetrical dunes and humpback dunes after Saunderson and Lockett, in press).

Asymmetrical dunes - Asymmetrical dunes typically had a short, steep lee side which formed an avalanche slope and a gentler, longer stoss side where erosion and bed transport took place (Fig. 6). This dune type was always found to be out of phase with the water surface. Total resistance to flow is the result of grain roughness and form roughness with the latter dominant. The most common mode of sediment transport is bed material load (considered by the author to be comprised of both bedload and saltating load). Individual grains roll up the stoss side of the dune and avalanche over the crest where they are deposited or stored. There they will remain until exposed by the downstream movement of the dune whereupon the cycle of moving up the back of the dune, avalanching and storage will be repeated. Thus, the movement of most of the bed material is in steps that are as long

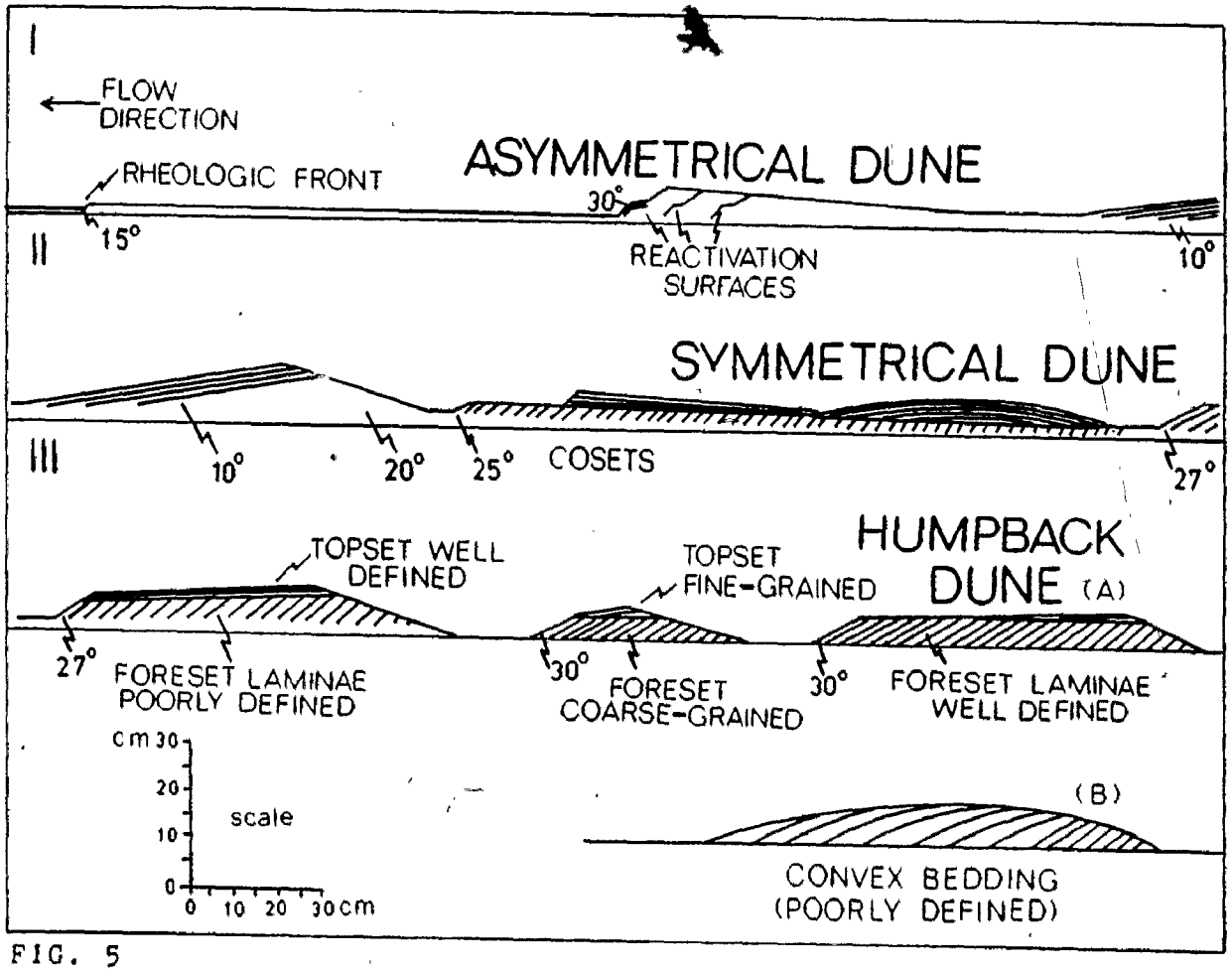

FIG. 5

Three morphological dune types formed: 1) asymmetrical, 2) symmetrical, and 3) humpback dunes. Panels I, II and III represent a continuous series of dunes formed in experimental run 9. Reactivation surfaces were cut by the reverse circulation which changed in size to the lee of asymmetrical dunes. Symmetrical dunes contained convex bedding and humpback dunes, topset and foreset bedding. Note that the maximum elevation on humpback dunes does not coincide with the tops of foreset slopes, and that one dune type may change to another (Panel III A, B).

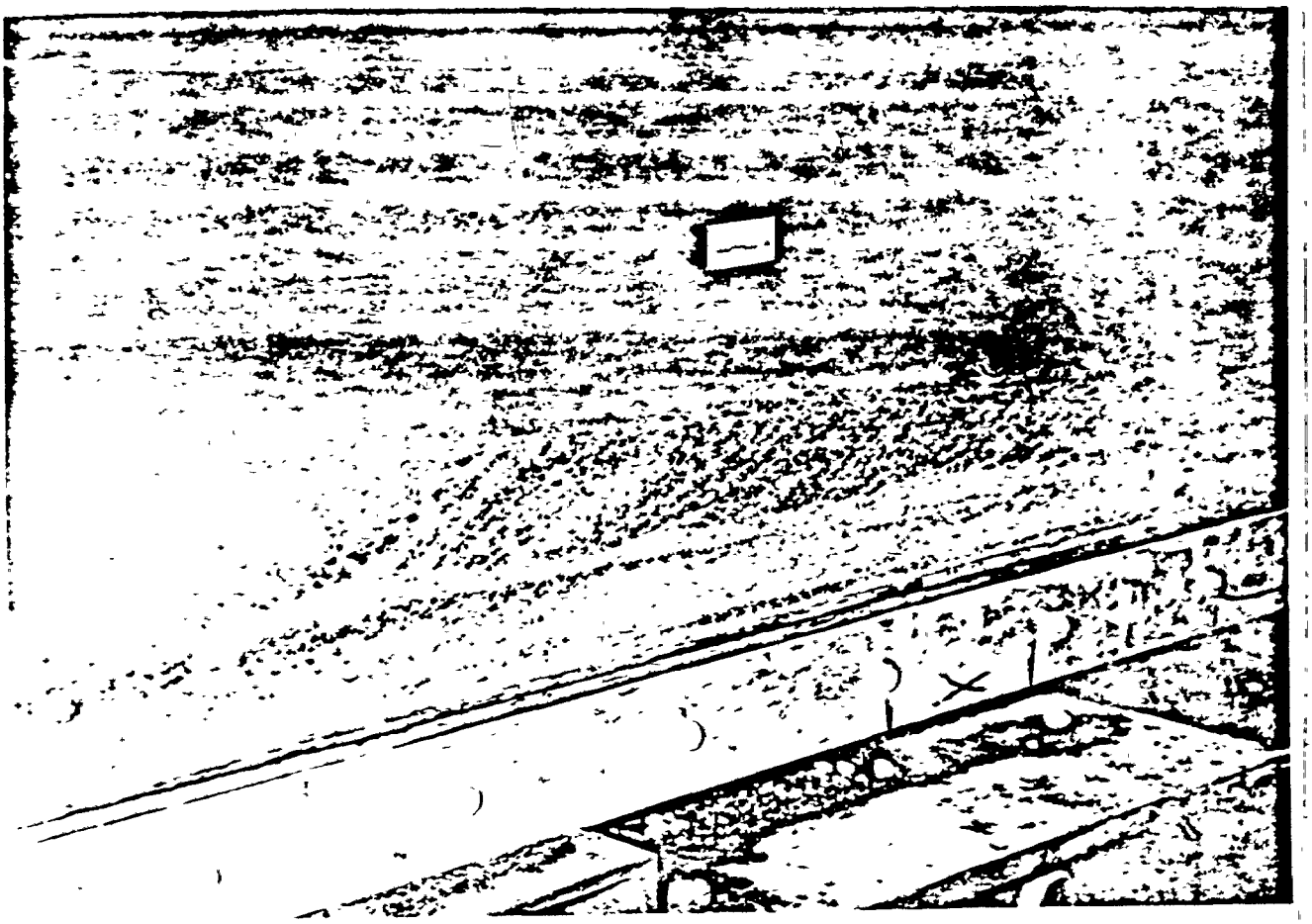

FIG. 6

Asymmetrical dune showing long, gentle stoss side which is erosional and transportational, and shorter, steeper lee side maintained by flow separation, reverse circulation and undermining. Cross-beds formed by avalanching (predominantly) and settling of suspended load through the zone of flow separation.

as the asymmetrical dune, with a time between steps dependent upon progradation or migration rates. Flow separation occurs at the crest of the asymmetrical dune and the zone of reverse circulation or backflow maintains the steepness of the avalanche slope by undermining it. Suspended load settles through the zone of flow separation to form bottomset laminae as is common for dunes and laboratory deltas (Jopling 1965a; Allen 1965, 1968a, 1968b) and backflow is often strong enough to form regressive ripples in the bottomset (Fig. 7). These ripples start to form at the point of flow reattachment and can be seen in profile to migrate upstream to the toe of the foreset and be preserved as underlying primary sedimentary structures as the dune profile migrates downstream.

The availability or frequency in arrival times of individual grains to the foreset crest determines avalanche frequency. As individual grains thicken and steepen the crest, a maximum slope is reached approximately equal to the angle of repose, the slope then fails and avalanching occurs. The maximum height to which the foreset slope of an asymmetrical dune may aggrade and the maximum length the lee slope may attain are also dependent on the availability of sediment for avalanching at the crest. If the dune is closely followed (less than 5 to 10 cm., approx.) by another dune of any type from upstream, or if a climbing coset overtakes the dune, the crest of the dune will receive substantially less sediment than it would otherwise receive and is starved, thus slowing or halting its aggradation and progradation rates.

Occasionally it was observed that the zone of reverse circulation or backflow decreased in thickness causing the upper half

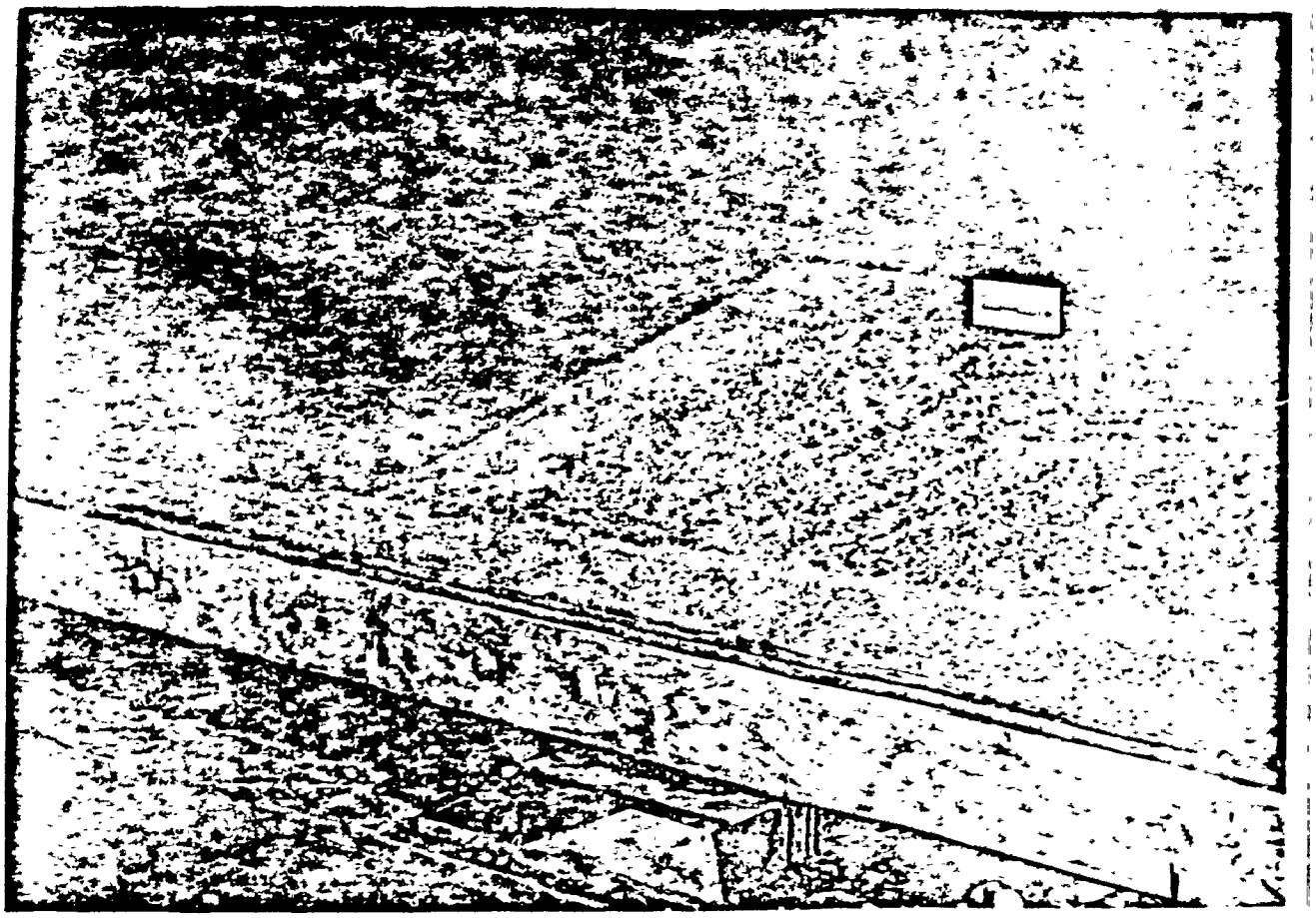

FIG.7

Asymmetrical dune resulting from transformation of humpback dune. Sigmoidal bedding inside the dune formed during humpback migration and continued during aggradation at the foreset during the change to the asymmetrical type. Note the bottomset deposition containing small, regressive ripples.

of the foreset slope of the asymmetrical dune to be eroded. The crest of the dune became planed off and a new crest formed slightly upstream from the first. Flow separation and avalanching of bed material load at the new crest produced a small set of cross-laminae superimposed on cross-stratification forming the dune, separated by a small erosion surface. Any cross strata with bedding structures greater than or equal to 1 cm. in thickness are considered to be cross-stratification and less than 1 cm. to be cross-lamination after McKee and Weir, 1953. This erosion surface is similar to the reactivation surfaces reported from the field investigations of modern streams (Collinson, 1970) but unlike larger streams, it is related to changes in the size of the separation zone to the lee of the dune crest rather than to erosion and renewed deposition as a consequence of changes in flow discharge. The observed mechanism was closer to that deduced by Jones and McCabe (1980, see their Fig. 5). The dune then grew in height, the separation zone became thicker and a single set of cross-laminae formed by avalanching along the lengthened foreset slope.

Convex dunes - Convex or symmetrical dunes (Fig. 8) were so designated because of their convex-upward profile as seen through the glass sidewalls of the flume. Upstream and downstream sides of this dune type were of equal steepness (symmetrical) and met at the highest point on the dune approximately halfway along its length. Flow separation was absent and consequently no undermining of the lee side took place. Convex, low-angle laminae were deposited to the lee of the crest but not by avalanching. Bed material load intermixed with suspended load was simply carried on over the crest by inertia and draped over the lee side. Cross-laminae were thus found to be poorly

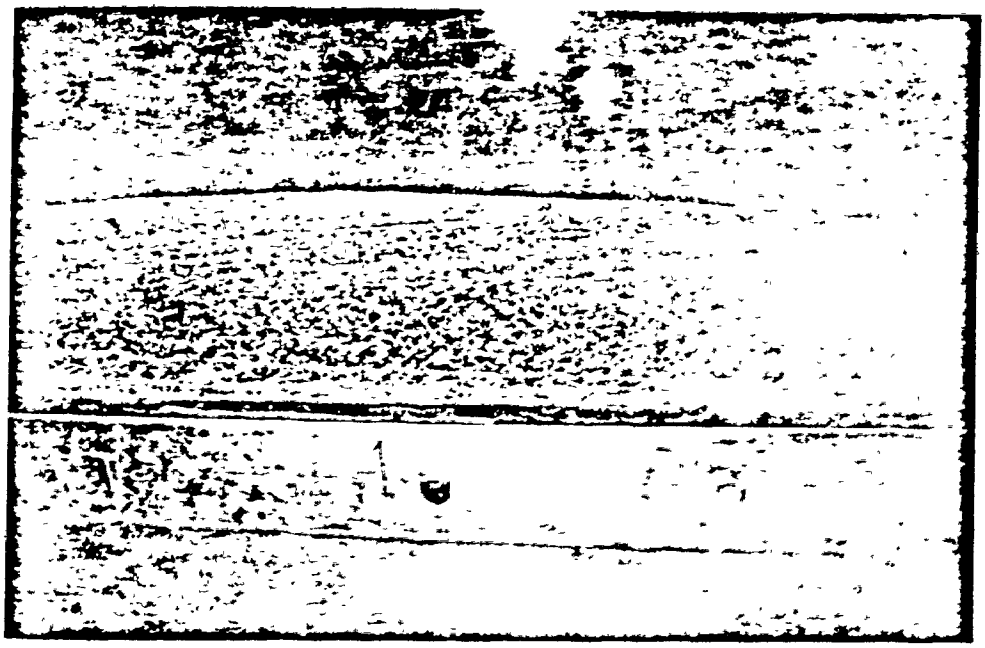

FIG. 8

Convex bedding preserved inside a humpback dune. The dune initially was a convex symmetrical dune displaying convex low-angled laminae and was transformed into a humpback dune.

sorted with poor bedding definition. This mode of deposition is very similar to that observed by Saunderson (1981) to the lee sides of antidunes in medium sands.

This dune type is considered to be a subsidiary bedform to the asymmetrical or humpback dune since it was not abundant in all runs or found in a series or dune train and was rarely seen to exist longer than the space of a couple of minutes before it was transformed into one of the other dune types.

At the beginning of experimental flume Runs #1 to 6 where relatively low Froude numbers were recorded (see Table 1), a small, convex mound of sediment was present on the flume's channel bottom. This mound, with no apparent bedding structure, was deposited at the head of the channel as artificial turbulent flow conditions were preferentially retarded by straightening baffles in the headbox. In this case, convex bedding was artificially initiated as sediment was draped over the lee of the highest point of the mound. However, as the mound thickened, the bedding became more angular and less convex. The dune rapidly acquired the shape, resistance to flow and sediment transport mechanisms typical of an asymmetrical dune.

Humpback dunes – Humpback dunes were considered the most unique dune structure generated by flows in the experiments (Fig. 5, III). These dunes differed greatly from both asymmetrical dunes and convex (symmetrical) dunes in that the point of maximum elevation was closer to the upstream limit of the dune rather than the middle as in convex dunes or the downstream avalanche as in asymmetrical dunes (Fig. 5). This dune type, unlike other bed configurations generated by flows in the lower flow regime, occasionally were observed to be in-phase or

just offset downstream from the water surface waves (Fig. 9). This near in-phase relationship of water surface to bed surface exemplifies the close proximity of this structure to those formed in-phase in the upper flow regime. The avalanche slope of the humpback dune was not observed to be a permanent feature and occasionally disappeared altogether or disappeared and then reformed. Erosion of the stoss side occurred up to the point of maximum height, the hump, but immediately downstream from this point, deposition from bed material load produced poorly sorted and poorly defined long, low-angled, almost horizontal lamination which extended when an avalanche slope existed, to its crest. The avalanche slope was much shorter than that of asymmetrical dunes, but like those dunes, it was maintained at a steep angle by backflow from flow separation. Like that of asymmetrical dunes, suspended load settled out through the zone of flow separation to form bottomset laminae and if backflow was strong enough, regressive ripples were formed in the bottomset. If the short foreset of the humpback dune atrophied, flow separation diminished as an effective sorting mechanism and sediment was essentially draped over the dune downstream from the hump. Sigmoidal bedding formed as topset or horizontal laminae merged uninterrupted with foreset bedding which in turn merged with bottomset bedding. It is this sigmoidal bedding which is considered to be the most distinctive structure found in humpback dunes.

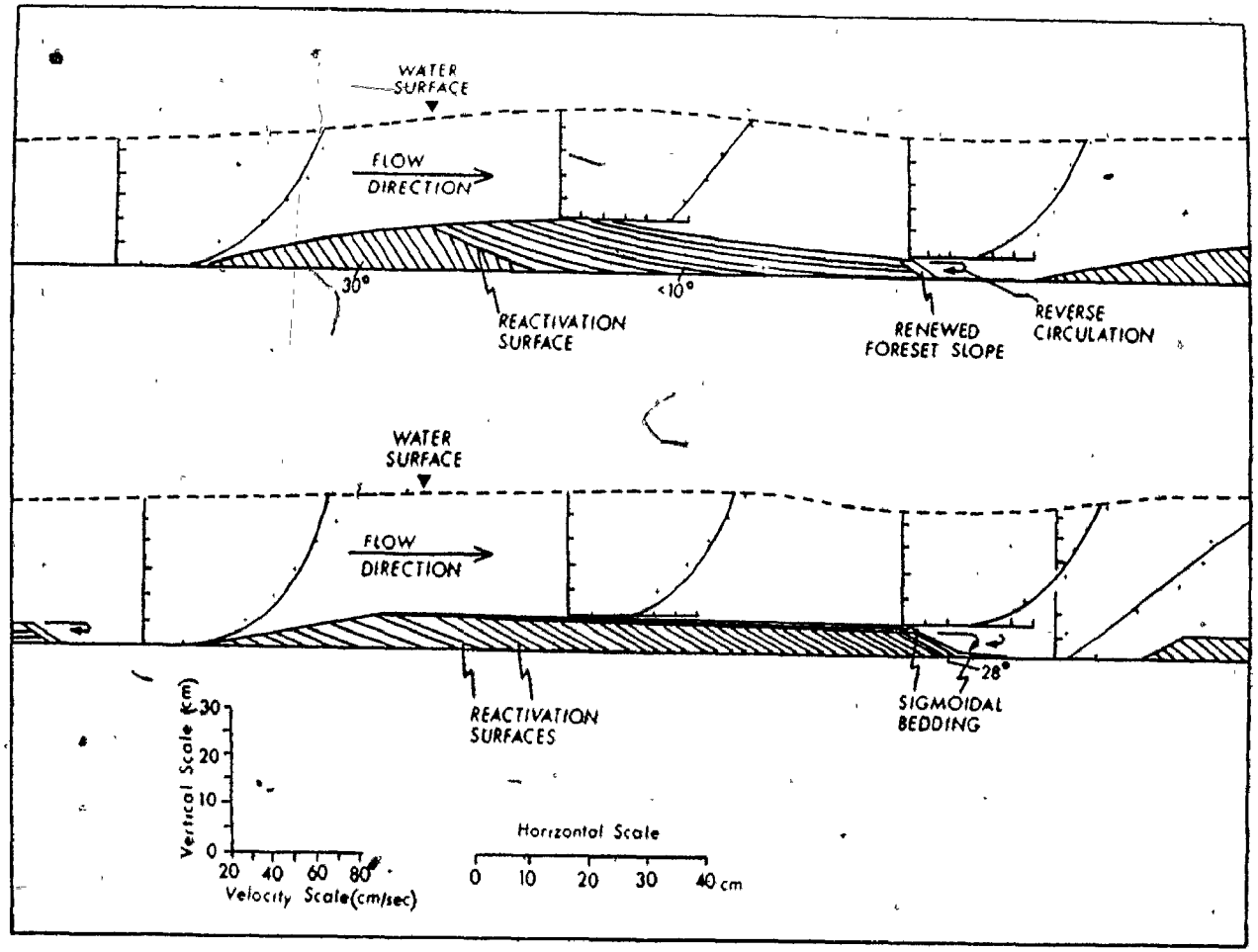

FIG. 9

Velocity profiles and phase relationships for humpback dunes. These dunes were formed in experimental run 9. The upper half of the diagram shows water surface wave and dune almost in phase. Each point on velocity profiles represents one velocity measured by pitot tube. Note the considerable shear (the velocity of the flow at the fluid-bed interphase) right at the bed at the locus of maximum elevation on the humpback profile (upper half of diagram, a velocity of 70 cm/sec) and the flow separation to the lee of each dune. In the lower half of the diagram, topset and foreset laminae are separated by an erosional surface, except at the front of the dune where they are continuous and grade into bottomsets (see FIG. 3) to form sigmoidal bedding.

4

RESULTS AND OBSERVATIONS ON BEDFORM DIMENSIONS, PRIMARY SEDIMENTARY STRUCTURES AND VELOCITY PROFILES OVER DUNES

In experimental flume Runs #1 to #6 both asymmetrical and humpback dunes were abundant and so it was possible to measure the dimensions of a number of dunes in each run as well as internal cross-stratification and migration or progradation rates (see Table 2). At higher Froude numbers (Runs #7 to #11) bed morphology was more intermixed and complex, so it was not possible to obtain meaningful average figures for bedform dimensions.

Average stoss side length ranged from about 76 cm. in Run #1 to 149 cm. in Run #3 and average lee side length from about 13 cm. in Run #1 to 17 cm. in Runs #2, 3 and 4. Dune amplitude varied from an average of about 6 cm. in Run #5 to 9 cm. in Runs #2, 3 and 4 and an average wavelength from 96 cm. in Run #1 to 160 cm. in Run #3. Steepness of foreset slopes ranged from 30^{o} in Run #6 to 36^{o} in Run #1 but mostly between 30^{o} to 33^{o}. Internal cross-stratification ranged from 29^{o} in Run #2 to 35^{o} in Run #3. Dune migration was slowest at about 2 cm./min. in Run #1 and fastest in Run #5 at about 11 cm./min. As opposed to what one would expect, there does not seem to be a good correlation between average slope of foresets and average slope of internal cross-stratification. However, the average slope of foresets do show a tendency to be steeper, probably reflecting the capacity of flow separation through backflow to reinforce and maintain the steep, angular

Table 2: Summary of Combined Average Dimensions and Migration Rates for Asymmetrical and Humpback Dunes for Experimental Flume Runs #1 to #6.*

RUN	AVERAGE WAVELENGTH (cm)	AVERAGE AMPLITUDE (cm)	AVERAGE LEE SIDE LENGTH (cm)	AVERAGE STOSS SIDE LENGTH (cm)	AVERAGE STEEPNESS OF FORESET SLOPE (degree^{o})	AVERAGE STEEPNESS OF INTERNAL CROSS - STRATIFICATION (degree^{o})	DUNE MIGRATION RATES PER MINUTE (cm)
1	96	8	13	76	36^{o}	33^{o}	1.7
2	105	9	17	90	32^{o}	29^{o}	2.5
3	160	9	17	143	33^{o}	35^{o}	4.6
4	125	9	17	105	31^{o}	30^{o}	3.6
5	120	6	11	110	31^{o}	32^{o}	10.8
6	105	8	15	80	30^{o}	30^{o}	6.8

*At higher flow velocities and Froude numbers, bed morphology was more intermixed and complex, so it was not possible to obtain meaningful average figures for bedform dimensions.

shape of the foresets.

Sediment size sorting occurred along the flume channel but not simply from coarse to medium in the downstream direction. Instead, sorting was made manifest by the presence of medium to fine, medium and coarse grained dunes (Fig. 4). The mechanical details of how this sorting came about were not obtainable from observation but it is certain that sorting was not an artifact of how the sediment was introduced because all size grades were thoroughly churned up using the bypass system near the end tank before being pumped along the return pipe to the headbox and into the open channel of the flume.

Primary sedimentary structures consisted of angular cross-stratification (dipping - 30^{o} - 35^{o}) inside asymmetrical dunes, convex to low-angle ($<20^{o}$ but mostly $\leq 10^{o}$) cross-lamination inside convex dunes and sigmoidal cross-lamination inside humpback dunes. The angular cross-strata of asymmetrical dunes were deposited as single sets and as cosets when the dune was overtaken by another. Cosets formed also when reactivation surfaces were cut and filled in association with changes in the size of the separation zone to the lee of dunes. In both single sets and cosets, the bedding was produced by intermittent avalanching of bed material load along the dune slip faces and by the suspended load which either settled through the separation zone or was plastered on the foreset slopes. Individual cross-beds, although the product of avalanching, were sometimes produced by a single avalanche or more commonly, by several short lived avalanches which reached only short distances down each foreset slope. If the frequency of avalanching was low (intermittently occurring) with a sufficient time interval between avalanches long enough to allow the grains to come to a

complete rest on the foreset or avalanche slip face the resulting cross-bed would show a vertical coarsening in grain sizes downward from the crest to the toe and inverse grading horizontally through the bed. The way by which grains sort themselves into different size distributions vertically down the foreset is probably closely associated with individual grain mass, where heavier, coarser grains roll and slide further down the foreset and are deposited nearer the toe, and lighter, finer grains closer to the crest. The process through which inverse grading occurs horizontally through the bed is not truly understood and is quite a speculative matter although dispersive pressure (Bagnold 1954, 1956; Jopling 1964) or another closely associated process seems likely. During the intervals between avalanching, smaller concentrations of fine particles of suspended load origin, carried by backflow, are continuously raining down or being deposited on the foreset slope. The cross-bedding of an asymmetrical dune resulting from such a combination of depositional processes as that discussed, is one of alternating thicker, coarse cross-beds of bed material load origin and thinner, fine cross-laminae of suspended load origin. Since these two kinds of cross-strata are deposited by different transport mechanisms, one would expect that the degree of sorting found in each would be quite different. Cross-stratified beds of bed material load origin should be found to be well sorted with respect to both the segregation of grain sizes between beds and grain size distributions within a bed. The bedding structure should also be darker in colour than cross-laminae, reflecting heavier mineral content and larger particles. Cross-laminated beds of suspended load origin should be found to be well sorted in respect to the segregation of grain sizes between laminae, since only one transport

mechanism was responsible for deposition, that being suspended load transport. Individual laminae should be found to be poorly sorted as a result of grains being plastered on the foreset by backflow without further sorting occurring.

If avalanching on the foreset slope is continuous or relatively frequent, grains moving down the slip face do not come to rest before being affected by continuing avalanche action, thus influencing their sorting ability. Particles from suspension carried by backflow are simultaneously deposited with the avalanching grains. If there is an appreciable amount of suspended load being deposited at the same time as the avalanching grains, the resulting cross-stratification would show poorly sorted beds with poor bedding definition.

Convex, symmetrical dunes, considered subsidiary bedforms of the asymmetrical and humpback dune varieties, have internal sedimentary structures comprising low-angled convex bedding (Fig. 8). Their morphological shape is thus one of a convex upward profile. Upstream and downstream slopes are of equal steepness as the result of high bed material load transport up the backs and over the tops (crest) without the sorting effects associated with flow separation. Because of this absence in flow separation and consequently backflow, bed material load and the coarsest fraction of suspended load near the bottom are intermixed and essentially draped over the lee side of these dunes by inertia without being segregated into two separate transport populations (as is the case immediately downstream of the foreset crests in asymmetrical dunes).Convex dunes were observed to form in experimental flume Runs #1 to #11 along with other dune types (in Run #12 only a plane bed was generated). However, due to the short span of time over

which convex dunes exist, only three were dimensionally documented, recorded and found in Runs #5, 9 and 11. For each of the individual dunes, the upstream and downstream slopes were of equal steepness and length, displaying a gentle convexing upward profile. However, the steepness, length of slope and dune thickness varied between dunes. The dunes from Run #9 and #11 had similar wavelengths of 60 cm. and 65 cm. with slopes of 10^{o} and 8^{o} and dune amplitudes of 10 cm. and 4 cm. The dune from Run #5 however, had a wavelength of 105 cm. and a slope of 20^{o} with an amplitude of 21 cm. Dune proximity and sediment availability were not considered a major factor in controlling the dimensions of these convex dunes since all three examples were located approximately the same distance between asymmetrical dunes and were all transformed in a matter of minutes into humpback dunes. Changes in convex dune dimensions were considered to be related more to variations in flow velocity where at a low flow velocity (Run #5) a convex dune may grow in amplitude and protrude into flow until a shear velocity is reached at the highest point on the bed which can erode the size class of material composing the dune. As the convex dune increases in amplitude, it also increases in wavelength although not proportionally. Thus once a critical shear velocity is met at the highest point on the dune bed, the dune will quickly cease to increase in dimensions.

Humpback dunes, unlike asymmetrical and convex, symmetrical dunes, are quite unique in that morphologically, the highest point on the structure is offset and closer to its upstream limit. As humpback dunes migrate down the flume channel, sigmoidal bedding forms but not all in one step. Rather, it forms in a series of steps of bedding developments. Erosion occurs on the upstream side of this dune type

and sediment is carried up to the point of maximum height, the hump at the top of the stoss side. Due to the absence of flow separation over the hump, sediment from bed material load and the coarser fraction of suspended load intermix and very thin (<5 cm.) low-angle laminae ($\leq 15^{o}$) are deposited as "topsets" from the hump and then prograde downstream to the top of the foreset slope as they thicken. If however, the hump of the dune protrudes high enough into flow, the shear at the bed will increase to such a point that as the coarse sediment from bed material load origins travels up and over the hump, the finer sized fractions will be thrown into suspension and the dune hump will be seen to "smoke". This coarse sediment held momentarily in suspension will then fall back to the bed a short distance downstream from the hump to form topsets as flow velocity decreases and flow depth increases. These topsets, composed of thin laminae of varying amounts of sediment from bed material and suspended load origin (depending on availability), are found to be poorly sorted and show poor bedding definition. Topsets may be seen to vary in thickness from a millimeter to as much as 5 cm. As topset laminae thicken and prograde to the foreset crest, sediment from bed material load origin quickly accumulates and then avalanches down the short foreset to form steeply dipping cross-laminae of approximately 30^{o} to 35^{o}. Avalanching on the foreset is usually of high frequency or is continuous and thus the resulting cross-laminae tend to be very thin (<5 cm.) and poorly sorted, displaying fair to poor bedding definition. These cross-laminae are deposited at the same time as bottomset laminae in the dune trough. However, since suspended load is usually not plentiful and if flow separation does exist, the size of the zone of reverse circulation is small, hence restricting the

ability of backflow to plaster sediments of suspended load origin (both from the bed and from suspension) on the foreset. Thus, cross-laminae of avalanche origin form an angular contact with the bottomset. The bottomset laminae are usually better sorted than topset or foreset laminae because of the small overall range of size distributions associated with suspended load. Since particles from suspension are continuously raining down in the trough locations and are not being deposited in discrete steps, bedding definition tends to be poor. Bottomsets are also seen to evenly decrease in thickness in the downstream direction from the toe of the foreset, probably reflecting an increase in competence of flow as it accelerates downstream from the trough, thereby reducing the ability of particles in suspension to settle out.

Sigmoidal bedding is thus seen to be the result of the fusion of topset deposition between the point of maximum height and the top of the foreset slope, foreset deposition by avalanching along the foreset slope and bottomset deposition in the bottom of the trough to the lee of the foreset. Although these three types of laminae are continuous, the topset laminae were much longer than either foreset or bottomset laminae, emphasizing a tendency for the dune top to lengthen and the foreset to shorten.

All three dune types, asymmetrical, convex and humpback, were often present in a single run and became transformed from one type to another of the three (Fig. 5). Convex dunes sometimes appeared as lower Froude numbers when only a small mound of sediment was present on the flume bottom, but then changed into asymmetrical dunes as the mound thickened (Fig. 10, I). Bedding then became more angular and less convex

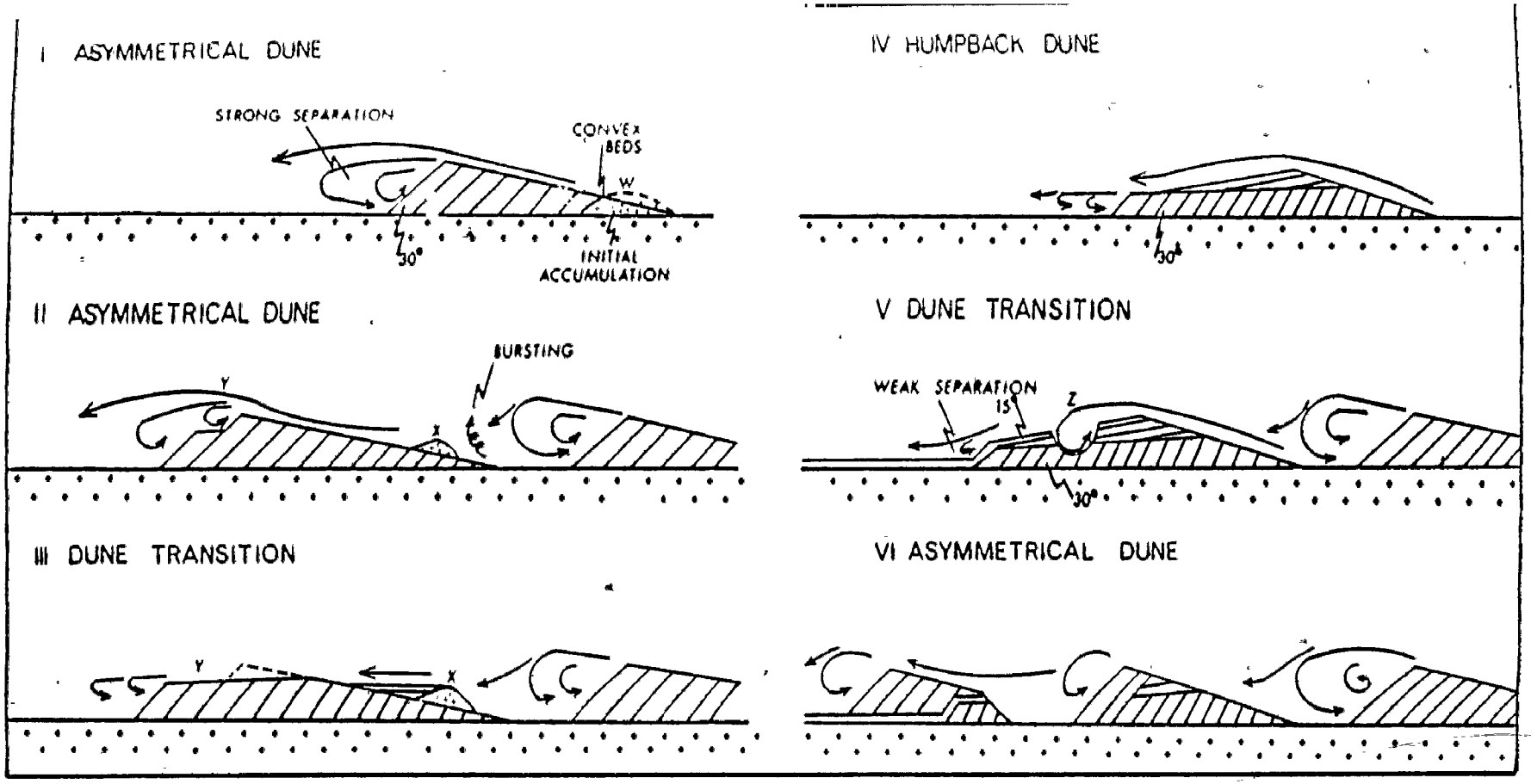

FIG. 10

Schematic diagram to show transitions asymmetrical dunes - humpback dune - asymmetrical dunes. A mound of sand forms a symmetrical, convex feature (I W) with convex bedding which then changes to steeper bedding as the sediment thickens and progrades. After asymmetrical dunes established (II), bursting occurred near the reattachment point and sediment thrown into suspension was deposited on the stoss side of a dune (X). Note storage of sediment near X forming toesets and erosion of upper foresets near Y to produce a humpback dune (IV). Topsets prograde forming sigmoidal bedding (V). Flow separation occurs (Z) and intensifies, dissecting the humpback into two separate (asymmetrical) dunes (VI). Run 11.

as the mound thickened. After asymmetrical dunes formed, flow separation and reattachment became distinguishable and near the point of reattachment (which oscillated rather than remaining stationary), bursting from the bed threw sediment temporarily into suspension. This sediment, being a mixture of bed material, was mostly too coarse to be held in suspension for any length of time and was deposited a short distance downstream on the stoss side of the same dune, thereby thickening the stoss side (Fig. 10, II). Bottom sediment comprised of bed material load which is normally deposited at the crest of the asymmetrical dune was now deposited to the lee of this mound forming parallel to almost horizontal cross-laminae. The height to which the crest may aggrade is dependent on the length of the lee slope which is determined by the amount of sediment available for avalanching at the crest. If this amount is insufficient to sustain the whole avalanche slope, the lower foreset progrades and the upper foreset either collapses or erodes (Fig. 10, III). In this way, the downstream end of the dune flattens and the stoss end thickens, resulting in a transformation from asymmetrical to humpback dunes (Fig. 10, IV). As the stoss end thickened, topset cross-laminae increased in length downstream to the shortened, avalanche slope and when flow separation on the foreset diminished as an effective sorting mechanism, sediment was draped over the foreset at a short distance downstream forming sigmoidal bedding. Velocity profiles indicate that bed shear stress was greatest near the highest point on a humpback dune as in one case from Run #9 where a near-bed velocity of about 70 cm./sec. was recorded (Fig. 9). But a short distance downstream from the highest point, flow separation was developed probably at a location where the

adverse pressure gradient reached a critical point and this separation eddy grew in size and intensity until the humpback dune became eroded into separate dunes, now asymmetrical (Fig. 10, VI).

At higher Froude numbers, the asymmetrical dunes atrophied to low amplitude features and rheological fronts (Moss, Walker and Hutka, 1980, p. 52-53) became more abundant on the bed which was almost plane. At lower Froude numbers, the water surface was out of phase with bed undulations, whereas at higher ones, they were either in phase or almost so (Fig. 9).

Two plane bed states were generated at two quite distinct Froude numbers in the experiments although both were formed in supercritical flows (Fr. $>$ 1). One was generated in Run #11 at a Froude number of 1.08. In this run, the Froude number was attained by increasing flow velocity through decreasing the hydraulic radius. Humpback dunes atrophied in the run to low amplitude features and rheological fronts became abundant on a bed which was flat. Humpback dunes, rheologic fronts and the plane bed were all found to be poorly sorted within individual laminae but well sorted between laminae and showed good bedding definition exemplified through alternating dark and light laminae of approximately 1 to 2 mm. in thickness. This plane bed generated was clearly associated with humpback dunes and is interpreted as being the upper stage plane bed found commonly at Froude numbers higher than dunes. Due to design limitations of the overshot tailgate, Froude numbers between 1.08 and 1.75 could not be attained. The second plane bed, generated at a Froude number of 1.75 in Run #12, had no other sedimentary structure associated with it other than parallel laminae composing the bed. The parallel laminae, like those generated at a

Froude number of 1.08 in Run #11, were poorly sorted within and well sorted between laminations and alternated from light to dark with a thickness of about 1 mm. This plane bed is different from the one generated in Run #11 and is probably more closely associated with plane beds observed at Froude numbers greater than those for in-phase waves (Williams, 1970).

Velocity Profiles Over Dunes

In order to investigate flow and form relationships more closely, 71 velocity profiles were constructed from pitot tube measurements of point velocities. Velocity profiles were recorded at specific locations from the bed upward to the surface of flow for a number of asymmetrical and humpback dunes. In order to allow for dune migration rates, the pitot tube was moved during the course of taking the profiles in order to keep the tube at the same location with respect to the dune profile. Four regressions; linear, logarithmic, exponential and power were calculated by computer (Hewlett-Packard HP-85, using their General Statistic Package) for each velocity profile and their coefficient of determination r^2 was used to identify the degree of fit (Table 3, Appendix B). In many instances, the r^2 value for different regressions are very close for the same velocity profile as seen for the exponents in exponential and power functions. However, in such cases, the larger r^2 value is considered to be the best fit of those equations fitted to the data.

Locations in dune troughs, halfway up stoss sides, "hump" and crests among others, were chosen in anticipation of a pattern emerging between location of a profile and the best fit relationship. As Table 3 (Appendix B) indicates, no such pattern resulted from the analysis. Power functions were the best fits for 34 of the 71 profiles,

exponential fits were the best for 16, linear fits for 20 and logarithmic the best fit for only one. Although the types of fit; linear, exponential and power, cannot be used as distinctive descriptors of flow profiles for specific locations on dune profiles, the values of the exponent in power fits do show a closer correlation with location. The highest values of the exponent in power function fits occur either on the backs of dunes or at the crests, whereas the values of exponents in trough areas are mostly much lower.

All of the linear fits show that considerable shear exists at the bed regardless of location and that the locus of zero velocity ($x = 0$) is inside the bed. A cautionary note must be added to this interpretation however, because it is often difficult to be certain that the pitot tube is right down at the bed when taking measurements, especially when the water is turbid. The locus of zero velocity is probably just below the fluid-sediment interface and thus could not be detected using the pitot tube available. For certain, values of about -50 (Table 3) cannot be used to predict the locus mathematically in a bed that was never more than about 25 cm. thick. The linear equations are obviously only valid over the data range measured.

The shape of velocity profiles over asymmetrical and humpback dunes were not found to be the same. Asymmetrical dunes had velocity profile shapes much like those shown by Bridge and Jarvis (1977) when bed shear was at a minimum in dune troughs and at a maximum near the dune crests. This distribution was not quite the same over humpback dunes. Least bed shear was again at trough locations but maximum bed shear occurred over the highest points, the humps, and then decreased slightly between the hump and the top of the avalanche slope (Fig. 9).

Maximum bed shear at the highest point was emphasized during experiments by intense sheet transport of bed load over the surface of the hump. In some dunes, when the hump became flattened, velocity profiles had more of a uniform shape over the tops of dunes or dune platforms (Fig. 9), showing a uniformity of fairly high bed shear such as is found over a plane bed.

5

DISCUSSION OF RESULTS

Simons and Richardson (1966, p. J11) described the bed configuration in the transition between lower and upper flow regimes as variable and dependant largely on antecedent conditions. If a bed were initially plane, then a decrease in stream power would result in a transitional bed configuration with many of the properties of a plane bed. However, an increase in power from an initial dune configuration would produce a transitional bed configuration with many of the characteristics of dunes. The same reasoning would seem to explain why the transitional forms discussed here have many of the structural attributes of dunes, because stream power was increased from the dune into the plane bed states (Table 1). Simons and Richardson (1966) describe dunes in the transition as becoming smaller in amplitude and longer in wavelength, longer and lower features did appear on the bed in the present runs (in Runs #9 and #10). However, measurements of wavelength and height did not in general show a progressive change as the Froude number increased. Instead, there were modal groupings of wavelengths and heights as well as considerable variance from Run #1 to #6 (Table 2) and when a plane bed developed at a higher Froude number (Run #11) the transition from dunes to plane bed was quite abrupt. Rather than progressively less steep foresets and cross-beds, bedding steepness remained mostly in the 30° to 35° range right up to the transition,

when a plane bed and rheological fronts became prominent. Convex, symmetrical dunes were found to be generated in all runs, #1 to #11, where stream power varied from subcritical ($Fr < 1$) in Runs #1 to #9 and supercritical ($Fr > 1$) in Runs #10 and #11. However, convex laminae of convex symmetrical dunes have very similar depositional origins as that of lee-side laminae of antidunes and standing waves.

The clearest analogy to rounding of asymmetrical and humpback dunes to form convex dunes in previous studies is rounding of ripples observed by Jopling and Forbes (1979) for the ripple to plane bed transition in a coarse silt. Jopling and Forbes observed that bed and water surfaces were sometimes in phase at the ripple to plane bed transition. One possibility is that similar morphological changes occur in the transition between bedforms of the lower flow regime and the lower stage plane bed of the upper flow regime regardless of whether these bedforms are dunes or ripples. Humpback bed undulations of much larger size than those reported here have been investigated in the Pitt River (Ashley, 1978) and dunes with convex-upward stoss sides have been found in the return pipes of the same flume as that used in the present study (McDonald and Vincent, 1972).

The in-phase relationship between some of the humpback dunes and water surface waves (Fig. 9; Run #9, Table 1), the presence of steeply dipping foresets, and the development of long plane beds on the tops of dunes exemplify the complexity that may occur at the transition from dunes to a plane bed and at the transition from subcritical to supercritical flow (Runs #9 to #11, Froude number close to 1.0). This complexity results from mixing of bed phases which is a normal

expectation near bed phase boundaries, particularly in quasi-equilibrium flows. Experiments of the present report are best considered quasi-equilibrium rather than truly equilibrium conditions, and the inherent, albeit small, unsteadiness of flow is probably related to the short recirculation time (5 to 6 hours) during each run.

Data from the author's experiments plotted on a velocity-size diagram after Middleton and Southard (1977) show dune configurations generated at flow conditions which are indicated to be more consistent with the development of a plane bed of the upper flow regime (Fig. 11). No doubt a transition exists where mixing of the dune and plane bed stability fields occur. Perhaps the boundary or transition zone separating the dune and plane bed fields occurs at higher velocities for medium to coarse sands.

Mixing of dune and plane bed phases is deducible for slightly unsteady, non-uniform flows from inspection of Allen and Leeder (1980, their Fig. 3) whose stability criteria separating ripple, dune and plane bed fields intersect, thus making it possible for more than one bedform to coexist as hydraulic and sediment transport conditions fluctuate slightly about some average, equilibrium intersection. Bridge (1981) considered the backs of dunes, when devoid of ripples, to be dynamically similar to upper regime plane beds. The long, nearly horizontal topset portions of humpback dunes are likewise considered to be plane beds which developed as a response to localized increases in velocity and shear at the bed. Morphologically, each forms a crestal platform like that shown diagramatically by Allen (1968a, p. 61) though unexplained by him at the time.

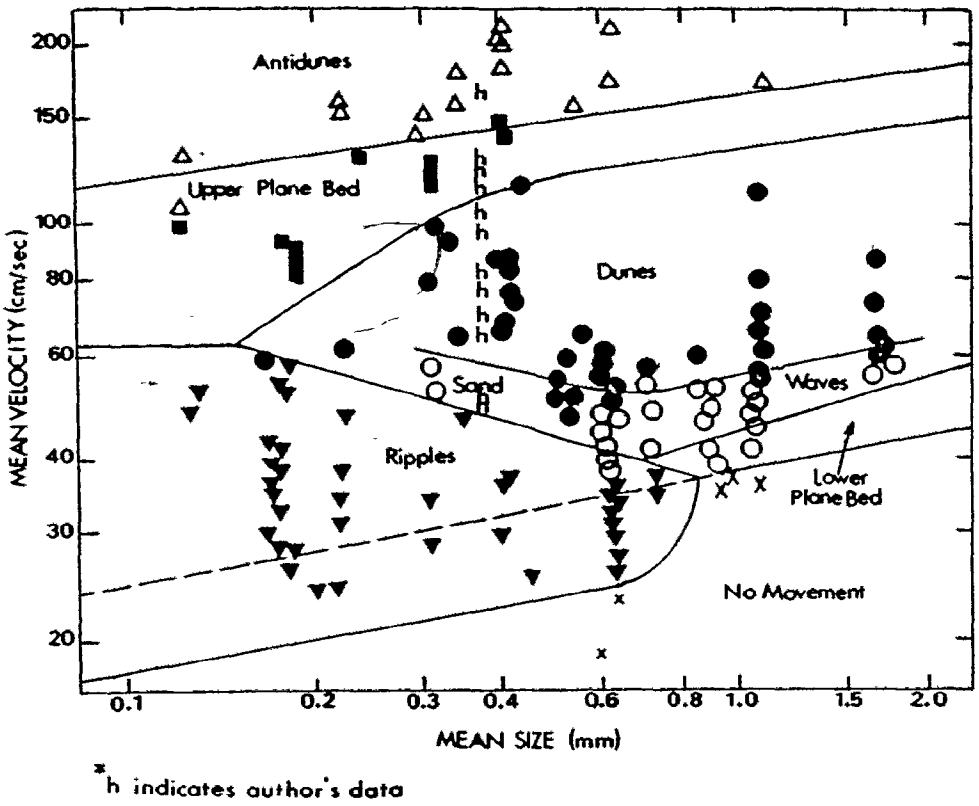

*h indicates author's data

FIG. 11

Velocity-size diagrams of plotted data from the experiments (see Table 1) with experimental data by L.A. Boguchwal (From Middleton and Southard, 1977, S.E.P.M. Short Course Notes 3, p. 7.37).

Sigmoidal bedding was the most distinctive structure found in the humpback dunes. This type of stratification has been reported from experiments on laboratory deltas (Jopling, 1965b, p. 789), hurricane washover deposits (Morton, 1978, his Fig. 7D), ancient point bar deposits (Nami and Leeder, 1978) and from linguoid ripples in modern flood deposits of ephemeral streams (Williams, 1971, p. 21). The structure was mentioned earlier (Davis, 1890, his Fig. 2) but without specific interpretation as a dune or sand wave structure. The relative lengths of the topset, foreset and bottomset segments of sigmoidal bedding probably reflect the proximity of conditions to the plane bed state. In other words, the foreset atrophies whereas the topset lengthens as the plane bed state is approached. As the foreset shortens, flow separation diminishes as an effective sorting mechanism and bottom load intermixed with suspended load is simply draped over the foreset slope, thereby rounding it off.

At the intermediate Froude numbers (Table 1) rheological fronts became an important mode of bed material load transport and by Runs #10 and #11 they became prevalent. At the lower Froude numbers they transported sediment along the backs and tops of dunes, delivering it to the upper foreset slope (where present). At higher Froude numbers, particularly at the onset of a plane bed, they became the normal mode of transport. At the highest Froude number of all (Run #12) discrete rheological fronts were no longer visible. The bed started to erode, although still plane, and diffuse clouds of eroded sediment migrated from upstream to downstream along the flume at the interface between fluid and bed. Current lineations were present in plan on the bed at this stage.

6

CONCLUSIONS

In the flume experiments conducted to investigate the transition between dune to plane bed state, three distinct dune configurations were generated in moderately sorted, medium to coarse sands. These were asymmetrical or triangular dunes, convex or symmetrical dunes and humpback dunes. Asymmetrical dunes contained single sets and cosets, the latter resulting from one dune overtaking another or because of changes in the size of the zone of flow separation. Cross-stratification and cross-lamination were steep (mostly 30° to 35°) and were formed largely by avalanching of bed material load along the foreset slopes and by sediment from suspension being plastered on the foreset slope by backflow. Convex, symmetrical dunes displayed convexing-upward profiles with lee and stoss slopes of equal length and steepness. Flow separation was absent over the highest point on the dune and consequently, sediment transport did not divide into two distinct populations. Sediment comprising bed material load and the coarsest fraction of suspended load were intermixed and draped over the lee-side of the dune by flow inertia forming poorly sorted, convex, low-angled, lee-side laminae. Humpback dunes differed from the two other dune types in that the highest point of elevation, the hump, was offset and closer to the upstream end of the structure. The short avalanche slope downstream from the hump was observed not to be

a permanent feature of this dune type, occasionally disappearing altogether or disappearing and then reforming. Erosion occurred on the stoss side up to the highest point on the hump and deposition to the lee of the hump formed sigmoidal bedding as the result of fusion between topset, foreset and bottomset laminae.

In the experiments, as the transition to a plane bed was approached from a dune configuration as stream power was increased, mixing took place of attributes from the dune stability field and from the plane bed field. Dune attributes consisted of cross-beds formed predominantly by avalanching which maintained fairly high dips (mostly 30° to 35°) due to flow separation right up to the transition from dunes to a plane bed. Attributes from the plane bed field consisted of low-angled to horizontal (parallel) laminae superimposed as topsets on dune forms. Overlapping of bed phases other than dunes and plane beds may have also occurred at the transition. The convex, symmetrical dunes with their convex, lee-side laminae are probably dynamically similar to in-phase waves (standing waves and antidunes), and indeed the in-phase nature of water surface and some humpback dunes is on the edge of the in-phase wave stability field.

The most distinctive structure of the experiments was the sigmoidal bedding found in humpback dunes. The relative lengths of the topset, foreset and bottomset portions of this type of bedding are direct results of the proximity of the dune-plane bed transition. Specifically, the topset component is relatively short and the foreset component is long at the low velocity end of the transition, whereas the foresets and bottomsets eventually disappear and the topset component lengthens and becomes dominant at the high velocity end

where a plane bed finally becomes the stable form.

The prime limitation of the experiments to investigate the transition of lower flow regime dunes to upper flow regime plane beds was the small overall range of attainable flow depth in each flume run which was never more than 45 cm. and was mostly between 20 and 40 cm. Due to shallow depth bedform dimensions may have been restricted and thus could have influenced bedforms and bedding structures to a degree. Further research is recommended into bed configurations generated in the transition from lower flow regime dunes to upper flow regime plane beds for various grain size distributions. This should aid in the development of more accurate stability diagrams as data becomes available for plotting. A better understanding of transitional bedforms and the overlapping of bed phase boundaries should be the result of such research. Continuing research into the transition between ripples and dunes of the lower flow regime and bed configurations of the upper flow regime for varying grain size distributions is recommended regardless of whether the lower flow regime structures are ripples or dunes since similar morphological changes probably occur in each. Finally there is a need to support the findings of experimental research conducted in the laboratory with sufficient examples of bedforms and bedding structures from the field generated under varying hydraulic and sediment transport conditions.

REFERENCES

Allen, J.R.L.,(1965), Sedimentation to the Lee of Small Underwater Sand Waves - An Experimental Study. J. Geol., v. 73, pp. 95-116.

Allen, J.R.L.,(1968a), Current Ripples, North Holland, Amsterdam, 433 p.

Allen, J.R.L.,(1968b), The Diffusion of Grains in the Lee of Ripples, Dunes and Sand Deltas. J. Sedim. Petrol., v. 38, pp. 621-633.

Allen, J.R.L. and M.R. Leeder,(1980), Criteria for the Instability of Upper-stage Plane Beds. Sedimentology, v. 27, pp. 209-217.

Ashley, G.M.,(1978), Bedforms in the Pitt River, British Columbia. In: Fluvial Sedimentology, (ed. by A.D. Miall), Can. Soc. Petrol. Geol. Mem. 5, pp.89-104.

Bagnold, R.A.,(1954), Experiments on a Gravity-free Dispersion of Large Solid Spheres in a Newtonian Fluid Under Shear. Proc. R. Soc. Lond., v. 255, pp. 49-63.

Bagnold, R.A.,(1956), The Flow of Cohesionless Grains in Fluid. Royal Soc. London Philos. Trans., v. 249, no. 964, pp. 235-297.

Banks, N.L. and J.D. Collinson,(1975), The Size and Shape of Small-scale Current Ripples: An Experimental Study Using Medium Sand. Sedimentology, v. 22, pp. 583-599.

Bridge, J.S.,(1981), Bed Shear Stress over Subaqueous Dunes, and the Transition to Upper-stage Plane Beds. Sedimentology, v. 28, pp.33-36.

Bridge, J.S. and J. Jarvis,(1977), Velocity Profiles and Bed Shear Stress over Various Bed Configurations in a River Bend. Earth Surface Processes, v. 2, pp. 281-294.

Collinson, J.D.,(1970), Bedforms of the Tana River, Norway. Geog. Annaler, v. 52, pp. 31-56.

Davis, W.M.,(1890), Structure and Origin of Glacial Sand Plains. Bul. Geol. Soc. Amer., v. 1, pp. 195-202.

Engelund, F. and J. Fredsøe,(1974), Transition from Dunes to Plane Bed in Alluvial Channels. Inst. Hydro., Hydraul., Eng., Tech. University of Denmark, Ser. Pap. 4.

Fahnestock, R.K.,(1963), Morphology and Hydrology of a Glacial Stream - White River, Mount Rainier, Washington. U.S. Geol. Surv., Prof. Pap., 422-A.

Gilbert, G.K.,(1914), Transportation of Debris by Running Water. U.S. Geol. Surv. Prof. Pap., 86.

Guy, H.P., D.B. Simons and E.V. Richardson,(1966), Summary of Alluvial Channel Data from Flume Experiments 1956-1961. U.S. Geol. Surv. Prof. Pap., 462-I.

Jones, C.M. and P.J. McCabe,(1980), Erosion Surfaces within Giant Fluvial Cross-beds of the Carboniferous in Northern England. J. Sedim. Petrol., v. 50, pp. 613-620.

Jopling, A.V.,(1964),Laboratory Study of Sorting Processes Related to Flow Separation. J. Geophys. Res., v. 69, pp. 3403-3418.

Jopling, A.V.,(1965a), Laboratory Study of the Distribution of Grain Size in Cross-bedded Deposits. In: Primary Sedimentary Structures and their Hydrodynamic Interpretation, (ed. by G.V. Middleton), Spec. Publ. Soc. Econ. Paleont. Miner., Tulsa, 12, pp. 53-65.

Jopling, A.V.,(1965b), Hydraulic Factors Controlling the Shape of Laminae in Laboratory Deltas. J. Sedim. Petrol., v. 35, pp. 777-791.

Jopling, A.V. and D.L. Forbes,(1979), Flume Study of Silt Transportation and Deposition. Geog. Annaler, v. 61A, pp. 67-85.

McDonald, B.C.,(1972), The Geological Survey of Canada Sedimentation Flume. Geol. Surv. Canada Pap., 71-46.

McDonald, B.C. and J.S. Vincent,(1972), Fluvial Sedimentary Structures Formed Experimentally in a Pipe, and their Implications for Interpretation of Subglacial Sedimentary Environments. Geol. Surv. Canada Pap., 72-27.

McKee, E.D. and G.W. Weir,(1953), Terminology for Stratification and Cross-stratification. Bul. Geol. Soc. Amer., v. 64. pp. 381-390.

Middleton, G.V., and J. Southard, (1977), Mechanics of Sediment Transport. S.E.P.M. Short Course Number 3, pp. 1-10.2.

Morton, R.A., (1978), Large-scale Rhomboid Bedforms and Sedimentary Structures Associated with Hurricane Washover. Sedimentology, v. 25, pp. 183-204.

Moss, A.J., P.H. Walker and J. Hutka, (1980), Movement of Loose, Sandy Detritus by Shallow Water Flows: An Experimental Study. Sed. Geol., v. 25, pp. 43-66.

Nami, M. and M.R. Leeder, (1978), Changing Channel Morphology and Magnitude in the Scalby Formation (M. Jurassic) of Yorkshire, England. In: Fluvial Sedimentology, (ed. by A.D. Miall), Can. Soc. Petrol. Geol. Mem. 5, pp. 431-440.

Saunderson, H.C., (1981), Tunnel Transformation of Antidunes. Physical Geography, v. 2, pp. 125-145.

Saunderson, H.C. and F.P.J. Lockett,(1981), Flume Experiments on the Dune-Plane Bed Transition. In: Modern and Ancient Fluvial Systems, Sedimentology and Processes, (Abstract), International Conference, University of Keele, Sept. 1981, p. 106.

Saunderson, H.C. and F.P.J. Lockett,(in press), Flume Experiments on Bedforms and Structures at the Dune-Plane Bed Transition. In: Modern and Ancient Fluvial Systems, (ed. by J.D. Collinson), International Assoc. Sediment., Spec. Pub.

Simons, D.B. and E.V. Richardson,(1962), Resistance to Flow in Alluvial Channels. Am. Soc. Civil Eng. Trans., v. 127, pt. 1, pp. 927-954.

Simons, D.B. and E.V. Richardson,(1963), Forms of Bed Roughness in Alluvial Channels. Am. Soc. Civil Eng. Trans., v. 128, pt. 1, pp. 284-302.

Simons, D.B. and E.V. Richardson,(1966), Resistance to Flow in Alluvial Channels. U.S. Geol. Surv., Prof. Pap. 422-J.

Simons, D.B., E.V. Richardson and M.L. Albertson,(1961), Flume Studies Using Medium Sands (0.45 mm.). U.S. Geol. Surv., Water Supply Pap. 1498-A.

Simons, D.B., E.V. Richardson and C.F. Nordin,(1965), Sedimentary Structures Formed by Flow in Alluvial Channels. In: Primary Sedimentary Structures and their Hydrodynamic Interpretation, (ed. by G.V. Middleton), Spec. Pub. Soc. Econ. Paleont. Miner., Tulsa, 12, pp. 34-52.

Sorby, H.C.,(1859), The Structures Produced by the Currents Present During the Deposition of Stratified Rocks. The Geologist, v. 2, pp. 137-147.

Southard, J.B.,(1971), Representation of Bed Configurations in Depth-Velocity-Size Diagrams. J. Sedim. Petrol., v. 41, pp. 903-915.

Southard, J.B. and L.A. Boguchwal,(1973), Flume Experiments on the Transition from Ripples to Lower Flat Bed with Increasing Grain Size. J. Sedim. Petrol., v. 42, pp. 1114-1121.

Williams, G.E.,(1971), Flood Deposits of the Sand-bed Ephemeral Streams of Central Australia. Sedimentology, v. 17, pp. 1-40.

Williams, G.P.,(1967), Flume Experiments on the Transport of a Coarse Sand. U.S. Geol. Surv. Prof. Pap., 562-B.

Williams, G.P.,(1970), Flume Width and Water Depth Effects in Sediment Transport Experiments. U.S. Geol. Surv. Prof. Pap., 562-H.

APPENDIX A

RESULTS OF GRAIN SIZE ANALYSIS FOR MEDIUM TO FINE, MEDIUM AND COARSE GRAINED DUNES.

Sieve Results for a Medium to Fine-Grained Dune
(Channel Sample of a Dune from Experimental Flume Run #4)

Dry Sample Weight = 46.7 gms.

Phi Value (Ø)	Weight Value (gms)	Weight Percent (%)	Cumulative Percent (%)
-1.0	0.27	0.60	0.60
-0.5	0.34	0.75	1.35
-0.0	0.64	1.40	2.75
+0.5	1.34	2.94	5.69
+1.0	5.65	12.41	18.10
+1.5	6.12	13.44	31.54
+2.0	9.93	21.81	53.35
+2.5	9.61	21.11	74.46
+3.0	8.51	18.69	93.15
+3.5	2.13	4.68	97.83
+4.0	0.91	1.99	99.82
Pan*	0.07	0.15	99.97

Passing Sample Weight = 45.52 gms.
Sieve Loss = 1.18 gms. or 2.53%

Sieving Time = 15 minutes

*Sediment size fractions finer than +4.0 Ø (Pan) are considered to be silts and clays and are too fine in nature to be conventionally sieved.

Sieve Results for a Medium-Grained Dune
(Channel Sample of a Dune from Experimental Flume Run #4)

Dry Sample Weight = 46.7 gms.

Phi Value (Ø)	Weight Value (gms)	Weight Percent (%)	Cumulative Percent (%)
-1.5	0.36	0.70	0.70
-1.0	0.58	1.12	1.82
-0.5	1.18	2.29	4.11
0.0	2.65	5.14	9.25
+0.5	4.12	7.98	17.23
+1.0	11.67	22.62	39.85
+1.5	8.62	16.71	56.56
+2.0	12.09	23.43	79.99
+2.5	5.67	11.00	90.99
+3.0	3.66	7.09	98.08
+3.5	0.66	1.28	99.36
+4.0	0.28	0.54	99.90
Pan*	0.03	0.06	99.96

Passing Sample Weight = 51.57 gms.
Sieve Loss = 0.03 gms. or 0.06%

Sieving Time = 15 minutes

*Sediment size fractions finer than +4.0 Ø (Pan) are considered to be silts and clays and are too fine in nature to be conventionally sieved.

Sieve Results for a Coarse-Grained Dune
(Channel Sample of a Dune from Experimental Flume Run #8)

Dry Sample Weight = 42.4 gms.

Phi Value (Ø)	Weight Value (gms)	Weight Percent (%)	Cumulative Percent (%)
-1.5	0.66	1.56	1.56
-1.0	1.75	4.13	5.69
-0.5	1.34	3.16	8.85
0.0	5.16	12.17	21.02
+0.5	7.81	18.42	39.44
+1.0	9.54	22.50	61.94
+1.5	10.44	24.62	86.56
+2.0	3.42	8.07	94.63
+2.5	0.92	2.17	96.80
+3.0	1.02	2.41	99.21
+3.5	0.08	0.19	99.40

Passing Sample Weight = 42.26 gms.
Sieve Loss = 0.14 gms. or 0.33%

Sieving Time = 15 minutes

APPENDIX B

METHODS AND RESULTS OF EQUATIONS TO SHOW BEST FITS FOR VELOCITY PROFILES.

Equations for Calculating Linear, Exponential, Logarithmic and Power Regressions and the Coefficient of Determination (r^2) for Each. (Calculated by a Hewlett-Packard HP-85 computer, using their General Statistic Package).

Table 3: Results of Regression Equation and their Coefficient of Determination for Velocity Profiles.

Equation for Calculating Linear Regression and the Coefficient of Determination (r^2).

y = flow depth; x = point velocity

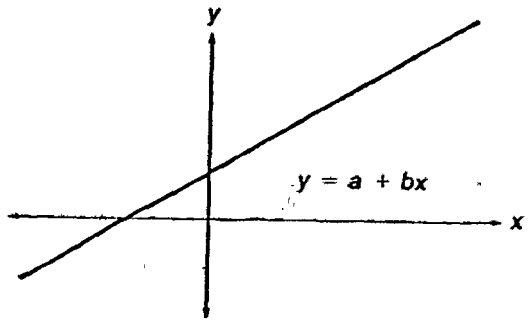

$$b = \frac{\Sigma x_i y_i - \frac{\Sigma x_i \Sigma y_i}{n}}{\Sigma x_i^2 - \frac{(\Sigma x_i)^2}{n}}$$

$$a = \left[\frac{\Sigma y_i}{n} - b \frac{\Sigma x_i}{n} \right]$$

$$r^2 = \frac{\left[\Sigma x_i y_i - \frac{\Sigma x_i \Sigma y_i}{n} \right]^2}{\left[\Sigma x_i^2 - \frac{(\Sigma x_i)^2}{n} \right] \left[\Sigma y_i^2 - \frac{(\Sigma y_i)^2}{n} \right]}$$

Equation for Calculating Exponential Regression and the Coefficient of Determination (r^2).

y = flow depth; x = point velocity

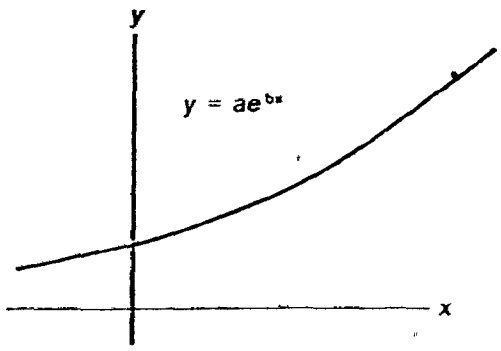

$$b = \frac{\Sigma x_i \ln y_i - \frac{1}{n}(\Sigma x_i)(\Sigma \ln y_i)}{\Sigma x_i^2 - \frac{1}{n}(\Sigma x_i)^2}$$

$$a = \exp\left[\frac{\Sigma \ln y_i}{n} - b\frac{\Sigma x_i}{n}\right]$$

$$r^2 = \frac{\left[\Sigma x_i \ln y_i - \frac{1}{n}\Sigma x_i \Sigma \ln y_i\right]^2}{\left[\Sigma x_i^2 - \frac{(\Sigma x_i)^2}{n}\right]\left[\Sigma(\ln y_i)^2 - \frac{(\Sigma \ln y_i)^2}{n}\right]}$$

Equation for Calculating Logarithmic Regression and the Coefficient of Determination (r^2).

y = flow depth; x = point velocity

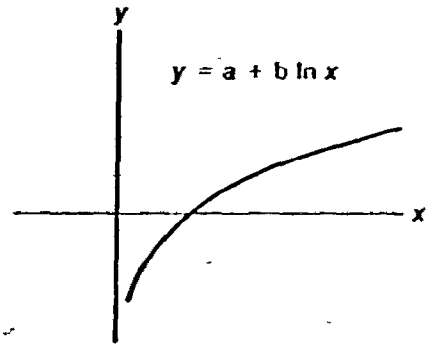

$$b = \frac{\Sigma y_i \ln x_i - \frac{1}{n} \Sigma \ln x_i \, \Sigma y_i}{\Sigma (\ln x_i)^2 - \frac{1}{n} (\Sigma \ln x_i)^2}$$

$$a = \frac{1}{n} (\Sigma y_i - b \, \Sigma \ln x_i)$$

$$r^2 = \frac{\left[\Sigma y_i \ln x_i - \frac{1}{n} \Sigma \ln x_i \, \Sigma y_i \right]^2}{\left[\Sigma (\ln x_i)^2 - \frac{1}{n} (\Sigma \ln x_i)^2 \right] \left[\Sigma y_i^2 - \frac{1}{n} (\Sigma y_i)^2 \right]}$$

Equation for Calculating Power Regression and the Coefficient of Determination (r^2).

y = flow depth; x = point velocity

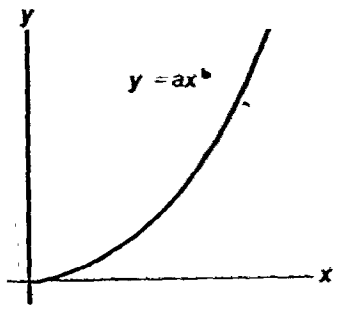

$$b = \frac{\Sigma(\ln x_i)(\ln y_i) - \frac{(\Sigma \ln x_i)(\Sigma \ln y_i)}{n}}{\Sigma(\ln x_i)^2 - \frac{(\Sigma \ln x_i)^2}{n}}$$

$$a = \exp\left[\frac{\Sigma \ln y_i}{n} - b\,\frac{\Sigma \ln x_i}{n}\right]$$

$$r^2 = \frac{\left[\Sigma(\ln x_i)(\ln y_i) - \frac{(\Sigma \ln x_i)(\Sigma \ln y_i)}{n}\right]^2}{\left[\Sigma(\ln x_i)^2 - \frac{(\Sigma \ln x_i)^2}{n}\right]\left[\Sigma(\ln y_i)^2 - \frac{(\Sigma \ln y_i)^2}{n}\right]}$$

Table 3: Regression Equations to Show Best Fits for Velocity Profiles Measured Midstream by Pitot Tube in Experiments.
y = flow depth; x = point velocity; origin of "y" and "x" axes is at the bed.

*a.d. = asymmetrical dune
h.d. = humpback dune

RUN #1

BED-FORM*	LOCATION OF VELOCITY PROFILE	LINEAR FIT	COEFFICIENT OF DETERMINATION (r^2)
a.d.	Dune trough	$y = -49.198 + 1.105x$	0.737
	Half-way up stoss side	$y = -9.333 + 0.467x$	0.717
	Dune crest	$y = -9.333 + 0.467x$	0.717
	Dune trough	$y = -18.953 + 0.753x$	0.897

		LOGARITHMIC FIT	COEFFICIENT OF DETERMINATION (r^2)
a.d.	Dune trough	$y = -233.594 + 61.537 \text{ Log}_e x$	0.691
	Half-way up stoss side	$y = -55.980 + 18.611 \text{ Log}_e x$	0.667
	Dune crest	$y = -55.980 + 18.611 \text{ Log}_e x$	0.667
	Dune trough	$y = -92.735 + 29.062 \text{ Log}_e x$	0.803

		EXPONENTIAL FIT	COEFFICIENT OF DETERMINATION (r^2)
a.d.	Dune trough	$y = 0.184 \exp(0.071x)$	0.932
	Half-way up stoss side	$y = 0.121 \exp(0.075x)$	0.744
	Dune crest	$y = 0.121 \exp(0.075x)$	0.744
	Dune trough	$y = 0.066 \exp(0.098x)$	0.815

RUN #1 con't.

BED-FORM*	LOCATION OF VELOCITY PROFILE	POWER FIT	COEFFICIENT OF DETERMINATION (r^2)
a.d.	Dune trough	$y = 0.0001(x^{4.046})$	0.906
	Half-way up stoss side	$y = 0.0001(x^{3.150})$	0.774
	Dune crest	$y = 0.0001(x^{3.150})$	0.774
	Dune trough	$y = 0.0001(x^{4.[illegible]})$	0.912

RUN #2

BED-FORM*	LOCATION OF VELOCITY PROFILE	LINEAR FIT	COEFFICIENT OF DETERMINATION (r^2)
h.d.	Dune trough	$y = -17.852 + 0.655x$	0.435
	Quarter-way up stoss side	$y = -35.981 + 0.974x$	0.795
	Upstream of crest	$y = -53.563 + 1.218x$	0.845
	Downstream of crest	$y = -66.611 + 1.406x$	0.776
a.d.	Dune crest	$y = -23.464 + 0.587x$	0.473
	Dune trough	$y = -10.902 + 0.564x$	0.580
		LOGARITHMIC FIT	COEFFICIENT OF DETERMINATION (r^2)
h.d.	Dune trough	$y = -98.435 + 29.534\ \mathrm{Log_e}x$	0.406
	Quarter-way up stoss side	$y = -173.768 + 48.125\ \mathrm{Log_e}x$	0.759
	Upstream of crest	$y = -233.195 + 61.837\ \mathrm{Log_e}x$	0.790
	Downstream of crest	$y = -290.444 + 75.417\ \mathrm{Log_e}x$	0.742
a.d.	Dune crest	$y = -108.867 + 29.776\ \mathrm{Log_e}x$	0.447
	Dune trough	$y = -58.157 + 20.053\ \mathrm{Log_e}x$	0.484
		EXPONENTIAL FIT	COEFFICIENT OF DETERMINATION (r^2)
h.d.	Dune trough	$y = 1.022\ \exp(0.047x)$	0.687
	Quarter-way up stoss side	$y = 0.008\ \exp(0.125x)$	0.703
	Upstream of crest	$y = 0.0001\ \exp(0.2x)$	0.920
	Downstream of crest	$y = 0.0001\ \exp(0.239x)$	0.910
a.d.	Dune crest	$y = 0.0001\ \exp(0.154x)$	0.961
	Dune trough	$y = 1.939\ \exp(0.038x)$	0.815

RUN #2 con't.

BED-FORM*	LOCATION OF VELOCITY PROFILE	POWER FIT	COEFFICIENT OF DETERMINATION (r^2)
h.d.	Dune trough	$y = 0.003(x^{2.160})$	0.658
	Quarter-way up stoss side	$y = 0.0001(x^{6.363})$	0.713
	Upstream of crest	$y = 0.001(x^{10.682})$	0.955
	Downstream of crest	$y = 0.001(x^{13.682})$	0.932
a.d.	Dune crest	$y = 0.0001(x^{8})$	0.950
	Dune trough	$y = 0.063(x^{1.416})$	0.732

RUN #3

BED-FORM*	LOCATION OF VELOCITY PROFILE	LINEAR FIT	COEFFICIENT OF DETERMINATION (r^2)
a.d.	Dune trough	$y = -20.923 + 0.656x$	0.807
	Half-way up stoss side	$y = -32.292 + 0.674x$	0.672
	Dune crest	$y = -21.238 + 0.510x$	0.644
	Dune trough	$y = -23.040 + 0.604x$	0.783
a.d.	Half-way up stoss side	$y = -78.789 + 1.415x$	0.770
	Dune crest	$y = -41.273 + 0.776x$	0.739
	Dune trough	$y = -23.742 + 0.802x$	0.804
		LOGARITHMIC FIT	COEFFICIENT OF DETERMINATION (r^2)
a.d.	Dune trough	$y = -111.760 + 32.311 \text{ Log}_e x$	0.708
	Half-way up stoss side	$y = -143.103 + 37.364 \text{ Log}_e x$	0.609
	Dune crest	$y = -94.632 + 25.930 \text{ Log}_e x$	0.565
	Dune trough	$y = -109.860 + 30.589 \text{ Log}_e x$	0.705
a.d.	Half-way up stoss side	$y = -352.545 + 87.807 \text{ Log}_e x$	0.741
	Dune crest	$y = -190.077 + 48.028 \text{ Log}_e x$	0.695
	Dune trough	$y = -135.763 + 39.523 \text{ Log}_e x$	0.706
		EXPONENTIAL FIT	COEFFICIENT OF DETERMINATION (r^2)
a.d.	Dune trough	$y = 1.232 \exp(0.041x)$	0.964
	Half-way up stoss side	$y = 0.0001 \exp(0.151x)$	0.998
	Dune crest	$y = 0.002 \exp(0.117x)$	0.990
	Dune trough	$y = 0.009 \exp(0.102x)$	0.903

RUN #3 con't.

BED-FORM*	LOCATION OF VELOCITY PROFILE	EXPONENTIAL FIT	COEFFICIENT OF DETERMINATION (r^2)
a.d.	Half-way up stoss side	$y = 0.0001 \exp(0.244x)$	0.925
	Dune crest	$y = 0.0001 \exp(0.163x)$	0.960
	Dune trough	$y = 2.474 \exp(0.036x)$	0.916
		POWER FIT	**COEFFICIENT OF DETERMINATION (r^2)**
a.d.	Dune trough	$y = 0.003(x^{2.109})$	0.914
	Half-way up stoss side	$y = 0.0001(x^{8.806})$	0.996
	Dune crest	$y = 0.0001(x^{6.304})$	0.983
	Dune trough	$y = 0.0001(x^{5.579})$	0.949
a.d.	Half-way up stoss side	$y = 0.0001(x^{15.603})$	0.948
	Dune crest	$y = 0.0001(x^{10.514})$	0.979
	Dune trough	$y = 0.013(x^{1.426})$	0.849

RUN #4

BED-FORM*	LOCATION OF VELOCITY PROFILE	LINEAR FIT	COEFFICIENT OF DETERMINATION (r^2)
a.d.	Dune trough	y = -7.969 + 0.539x	0.669
	Half-way up stoss side	y = -19.862).621x	0.385
	Dune crest	y = -32.316 + 0.732x	0.492
	Dune trough	y = -11.313 + 0.617x	0.794
a.d.	Half-way up stoss side	y = -54.628 + 1.217x	0.861
	Dune crest	y = -26.772 + 0.691x	0.662
	Dune trough	y = -19.846 + 0.690x	0.666

		LOGARITHMIC FIT	COEFFICIENT OF DETERMINATION (r^2)
a.d.	Dune trough	y = -42.052 + 16.364 $Log_e x$	0.520
	Half-way up stoss side	y = -111.9001 + 31.76 $Log_e x$	0.388
	Dune crest	y = -143.930 + 38.407 $Log_e x$	0.452
	Dune trough	y = -54.229 + 19.886 $Log_e x$	0.601
a.d.	Half-way up stoss side	y = -261.04 + 68.516 $Log_e x$	0.841
	Dune crest	y = -115.064 + 32.103 $Log_e x$	0.579
	Dune trough	y = -97.709 + 29.456 $Log_e x$	0.566

		EXPONENTIAL FIT	COEFFICIENT OF DETERMINATION (r^2)
a.d.	Dune trough	y = 2.6001 exp(0.035x)	0.856
	Half-way up stoss side	y = 0.002 exp(0.139x)	0.786
	Dune crest	y = 0.0001 exp(0.160x)	0.957
	Dune trough	y = 2.558 exp(0.036x)	0.955

RUN #4 con't.

BED-FORM*	LOCATION OF VELOCITY PROFILE	EXPONENTIAL FIT	COEFFICIENT OF DETERMINATION (r^2)
a.d.	Half-way up stoss side	$y = 0.001 \exp(0.051x)$	0.715
	Dune crest	$y = 0.002 \exp(0.132x)$	0.982
	Dune trough	$y = 1.216 \exp(0.045x)$	0.845
		POWER FIT	COEFFICIENT OF DETERMINATION (r^2)
a.d.	Dune trough	$y = 0.217(x^{1.131})$	0.754
	Half-way up stoss side	$y = 0.0001(x^{7.383})$	0.849
	Dune crest	$y = 0.0001(x^{8.733})$	0.947
	Dune trough	$y = 0.152(x^{1.233})$	0.836
a.d.	Half-way up stoss side	$y = 0.0001\ (x^{0.741})$	0.741
	Dune crest	$y = 0.0001(x^{6.590})$	0.988
	Dune trough	$y = 0.006(x^{1.987})$	0.781

RUN #5

BED-FORM*	LOCATION OF VELOCITY PROFILE	LINEAR FIT	COEFFICIENT OF DETERMINATION (r^2)
a.d.	Dune trough	$y = -18.438 + 0.529x$	0.982
	Quarter-way up stoss side	$y = -22.378 + 0.573x$	0.919
	Half-way up stoss side	$y = -19.722 + 0.501x$	0.930
	Quarter-way from crest	$y = -32.502 + 0.576x$	0.943
	Dune crest	$y = -13.064 + 0.329x$	0.710
	Dune trough	$y = -49.370 + 0.886x$	0.923
a.d.	Half-way up stoss side	$y = -37.186 + 0.613x$	0.878
	Dune crest	$y = -12.359 + 0.298x$	0.765

		LOGARITHMIC FIT	COEFFICIENT OF DETERMINATION (r^2)
a.d.	Dune trough	$y = -118.473 + 32.468 \text{ Log}_e x$	0.945
	Quarter-way up stoss side	$y = -113.443 + 31.036 \text{ Log}_e x$	0.854
	Half-way up stoss side	$y = -96.330 + 26.388 \text{ Log}_e x$	0.851
	Quarter-way from crest	$y = -186.854 + 45.858 \text{ Log}_e x$	0.934
	Dune crest	$y = -61.508 + 17.248 \text{ Log}_e x$	0.616
	Dune trough	$y = -274.880 + 67.749 \text{ Log}_e x$	0.894
a.d.	Half-way up stoss side	$y = -179.511 + 43.839 \text{ Log}_e x$	0.825
	Dune crest	$y = -58.889 + 16.399 \text{ Log}_e x$	0.651

RUN #5 con't.

BED-FORM*	LOCATION OF VELOCITY PROFILE	EXPONENTIAL FIT	COEFFICIENT OF DETERMINATION (r^2)
a.d.	Dune trough	$y = 1.174 \exp(0.037x)$	0.981
	Quarter-way up stoss side	$y = 0.01 \exp(0.101x)$	0.842
	Half-way up stoss side	$y = 0.005 \exp(0.109x)$	0.891
	Quarter-way from crest	$y = 0.286 \exp(0.046x)$	0.944
	Dune crest	$y = 0.007 \exp(0.087x)$	0.997
	Dune trough	$y = 0.546 \exp(0.045x)$	0.954
a.d.	Half-way up stoss side	$y = 0.0001 \exp(0.139x)$	0.913
	Dune crest	$y = 0.011 \exp(0.075x)$	0.991

		POWER FIT	COEFFICIENT OF DETERMINATION (r^2)
a.d.	Dune trough	$y = 0.001(x^{2.363})$	0.998
	Quarter-way up stoss side	$y = 0.0001(x^{5.934})$	0.918
	Half-way up stoss side	$y = 0.0001(x^{6.206})$	0.958
	Quarter-way from crest	$y = 0.0001(x^{3.739})$	0.961
	Dune crest	$y = 0.0001(x^{4.854})$	0.993
	Dune trough	$y = 0.0001(x^{3.469})$	0.947
a.d.	Half-way up stoss side	$y = 0.0001(x^{10.435})$	0.951
	Dune crest	$y = 0.0001(x^{4.5})$	0.998

RUN #6

BED-FORM*	LOCATION OF VELOCITY PROFILE	LINEAR FIT	COEFFICIENT OF DETERMINATION (r^2)
a.d.	Dune trough	$y = -16.443 + 0.502x$	0.929
	Dune crest	$y = -76.684 + 1.161x$	0.975
Coset	Half-way up stoss side	$y = -50.671 + 0.880x$	0.952
	Dune crest	$y = -90.308 + 1.312x$	0.944
	Dune trough	$y = -15.918 + 0.515x$	0.777
Coset	Half-way up stoss side	$y = -61.427 + 1.097x$	0.964
	Dune crest	$y = -54.332 + 1.002x$	0.870
	Dune trough	$y = -11.701 + 0.481x$	0.712

		LOGARITHMIC FIT	COEFFICIENT OF DETERMINATION (r^2)
a.d.	Dune trough	$y = -86.984 + 25.016 \text{ Log}_e x$	0.853
	Dune crest	$y = -369.769 + 88.194 \text{ Log}_e x$	0.958
Coset	Half-way up stoss side	$y = -246.625 + 60.840 \text{ Log}_e x$	0.919
	Dune crest	$y = -428.774 + 101.290 \text{ Log}_e x$	0.928
	Dune trough	$y = -65.864 + 20.352 \text{ Log}_e x$	0.627
Coset	Half-way up stoss side	$y = -294.521 + 73.09 \text{ Log}_e x$	0.945
	Dune crest	$y = -263.565 + 65.898 \text{ Log}_e x$	0.861
	Dune trough	$y = -46.554 + 16.003 \text{ Log}_e x$	0.567

		EXPONENTIAL FIT	COEFFICIENT OF DETERMINATION (r^2)
a.d.	Dune trough	$y = 0.031 \exp(0.087x)$	0.821
	Dune crest	$y = 0.0001 \exp(0.192x)$	0.787

RUN #6 con't.

BED-FORM*	LOCATION OF VELOCITY PROFILE	EXPONENTIAL FIT	COEFFICIENT OF DETERMINATION (r^2)
Coset	Half-way up stoss side	$y = 0.0001 \exp(0.152x)$	0.831
	Dune crest	$y = 0.0001 \exp(0.223x)$	0.804
	Dune trough	$y = 0.025 \exp(0.09x)$	0.968
Coset	Half-way up stoss side	$y = 0.0001 \exp(0.182x)$	0.776
	Dune crest	$y = 0.0001 \exp(0.168x)$	0.721
	Dune trough	$y = 0.043 \exp(0.088x)$	0.961
		POWER FIT	COEFFICIENT OF DETERMINATION (r^2)
a.d.	Dune trough	$y = 0.0001(x^{4.777})$	0.915
	Dune crest	$y = 0.0001(x^{15.08})$	0.824
Coset	Half-way up stoss side	$y = 0.0001(x^{10.988})$	0.882
	Dune crest	$y = 0.0001(x^{17.079})$	0.832
	Dune trough	$y = 0.0001(x^{4.034})$	0.998
Coset	Half-way up stoss side	$y = 0.0001(x^{12.589})$	0.824
	Dune crest	$y = 0.0001(x^{11.321})$	0.748
	Dune trough	$y = 0.0001(x^{3.322})$	0.989

RUN #7

BED-FORM*	LOCATION OF VELOCITY PROFILE	LINEAR FIT	COEFFICIENT OF DETERMINATION (r^2)
h.d.	Dune trough	$y = -9.571 + 0.272x$	0.385
	Half-way up stoss side	$y = -30.428 + 0.451x$	0.915
	Dune crest	$y = -47.447 + 0.582x$	0.957
	Dune trough	$y = -22.864 + 0.429x$	0.807
h.d.	Half-way up stoss side	$y = -20.118 + 0.364x$	0.876
	Dune crest	$y = -37.833 + 0.493x$	0.825
	Dune trough	$y = -27.933 + 0.552x$	0.834
		LOGARITHMIC FIT	COEFFICIENT OF DETERMINATION (r^2)
h.d.	Dune trough	$y = -83.702 + 22.006 \text{ Log}_e x$	0.411
	Half-way up stoss side	$y = -154.314 + 36.667 \text{ Log}_e x$	0.880
	Dune crest	$y = -240.572 + 54.658 \text{ Log}_e x$	0.935
	Dune trough	$y = -132.821 + 33.119 \text{ Log}_e x$	0.770
h.d.	Half-way up stoss side	$y = -114.135 + 28.275 \text{ Log}_e x$	0.857
	Dune crest	$y = -194.751 + 44.856 \text{ Log}_e x$	0.814
	Dune trough	$y = -183.408 + 45.612 \text{ Log}_e x$	0.838
		EXPONENTIAL FIT	COEFFICIENT OF DETERMINATION (r^2)
h.d.	Dune trough	$y = 1.161 \exp(0.027x)$	0.577
	Half-way up stoss side	$y = 0.0001 \exp(0.124x)$	0.909
	Dune crest	$y = 0.0001 \exp(0.153x)$	0.869
	Dune trough	$y = 0.481 \exp(0.037x)$	0.948

RUN #7 con't.

BED-FORM*	LOCATION OF VELOCITY PROFILE	EXPONENTIAL FIT	COEFFICIENT OF DETERMINATION (r^2)
h.d.	Half-way up stoss side	$y = 0.005 \exp(0.082x)$	0.591
	Dune crest	$y = 0.0001 \exp(0.139x)$	0.863
	Dune trough	$y = 1.056 \exp(0.033x)$	0.815
		POWER FIT	COEFFICIENT OF DETERMINATION (r^2)
h.d.	Dune trough	$y = 0.001(x^{2.152})$	0.608
	Half-way up stoss side	$y = 0.0001(x^{10.457})$	0.943
	Dune crest	$y = 0.0001(x^{14.796})$	0.903
	Dune trough	$y = 0.0001(x^{2.922})$	0.928
h.d.	Half-way up stoss side	$y = 0.0001(x^{6.474})$	0.592
	Dune crest	$y = 0.0001(x^{12.904})$	0.889
	Dune trough	$y = 0.0001(x^{2.785})$	0.832

RUN #8

BED-FORM*	LOCATION OF VELOCITY PROFILE	LINEAR FIT	COEFFICIENT OF DETERMINATION (r^2)
h.d.	Dune trough	$y = -2.487 + 0.192x$	0.840
	Dune crest	$y = -23.001 + 0.420x$	0.924
	Dune trough	$y = -12.317 + 0.333x$	0.953
	Half-way up stoss side	$y = -75.575 + 1.092x$	0.985
	Dune crest	$y = -6.156 + 0.213x$	0.854
	Dune trough	$y = -10.059 + 0.305x$	0.894
		LOGARITHMIC FIT	COEFFICIENT OF DETERMINATION (r^2)
h.d.	Dune trough	$y = -28.231 + 9.853 \text{ Log}_e x$	0.749
	Dune crest	$y = -123.712 + 30.919 \text{ Log}_e x$	0.878
	Dune trough	$y = -70.747 + 19.635 \text{ Log}_e x$	0.859
	Half-way up stoss side	$y = -370.261 + 87.271 \text{ Log}_e x$	0.982
	Dune crest	$y = -30.329 + 9.64 \text{ Log}_e x$	0.711
	Dune trough	$y = -66.592 + 18.722 \text{ Log}_e x$	0.850
		EXPONENTIAL FIT	COEFFICIENT OF DETERMINATION (r^2)
h.d.	Dune trough	$y = 0.342 \exp(0.036x)$	0.608
	Dune crest	$y = 0.003 \exp(0.089x)$	0.846
	Dune trough	$y = 0.035 \exp(0.068x)$	0.818
	Half-way up stoss side	$y = 0.0001 \exp(0.197x)$	0.653
	Dune crest	$y = 0.037 \exp(0.063x)$	0.970
	Dune trough	$y = 0.079 \exp(0.058x)$	0.659

RUN #8 con't.

BED-FORM*	LOCATION OF VELOCITY PROFILE	POWER FIT	COEFFICIENT OF DETERMINATION (r^2)
h.d.	Dune trough	$y = 0.002(x^{1.890})$	0.560
	Dune crest	$y = 0.0001(x^{6.976})$	0.910
	Dune trough	$y = 0.0001(x^{4.568})$	0.946
	Half-way up stoss side	$y = 0.0001(x^{16.044})$	0.676
	Dune crest	$y = 0.0001(x^{3.147})$	0.999
	Dune trough	$y = 0.0001(x^{3.720})$	0.683

RUN #9

BED-FORM*	LOCATION OF VELOCITY PROFILE	LINEAR FIT	COEFFICIENT OF DETERMINATION (r^2)
h.d.	Dune trough	$y = -11.844 + 0.291x$	0.907
	Half-way up stoss side	$y = -38.918 + 0.561x$	0.978
	Dune crest	$y = -13.955 + 0.321x$	0.747
	Dune trough	$y = -19.751 + 0.409x$	0.919
h.d.	Half-way up stoss side	$y = -13.360 + 0.341x$	0.928
	Dune crest	$y = -14.145 + 0.301x$	0.812
	Dune trough	$y = -9.029 + 0.35x$	0.882
		LOGARITHMIC FIT	COEFFICIENT OF DETERMINATION (r^2)
h.d.	Dune trough	$y = -62.251 + 17.198 \text{ Log}_e x$	0.785
	Half-way up stoss side	$y = -212.544 + 49.964 \text{ Log}_e x$	0.972
	Dune crest	$y = -66.467 + 18.138 \text{ Log}_e x$	0.642
	Dune trough	$y = -104.187 + 27.130 \text{ Log}_e x$	0.823
h.d.	Half-way up stoss side	$y = -69.144 + 19.164 \text{ Log}_e x$	0.815
	Dune crest	$y = -70.565 + 18.778 \text{ Log}_e x$	0.705
	Dune trough	$y = -58.530 + 17.813 \text{ Log}_e x$	0.755
		EXPONENTIAL FIT	COEFFICIENT OF DETERMINATION (r^2)
h.d.	Dune trough	$y = 0.026 \exp(0.065x)$	0.915
	Half-way up stoss side	$y = 0.0001 \exp(0.104x)$	0.685
	Dune crest	$y = 0.007 \exp(0.082x)$	0.980
	Dune trough	$y = 0.014 \exp(0.074x)$	0.880

RUN #9 con't.

BED-FORM*	LOCATION OF VELOCITY PROFILE	EXPONENTIAL FIT	COEFFICIENT OF DETERMINATION (r^2)
h.d.	Half-way up stoss side	$y = 0.02 \exp(0.074x)$	0.900
	Dune crest	$y = 0.009 \exp(0.073x)$	0.971
	Dune trough	$y = 0.276 \exp(0.048x)$	0.482
		POWER FIT	COEFFICIENT OF DETERMINATION (r^2)
h.d.	Dune trough	$y = 0.0001(x^{4.271})$	0.985
	Half-way up stoss side	$y = 0.0001(x^{9.600})$	0.730
	Dune crest	$y = 0.0001(x^{4.991})$	0.989
	Dune trough	$y = 0.0001(x^{5.401})$	0.960
h.d.	Half-way up stoss side	$y = 0.0001(x^{4.656})$	0.978
	Dune crest	$y = 0.0001(x^{4.948})$	0.997
	Dune trough	$y = 0.0001(x^{2.387})$	0.399

RUN #10

BED-FORM*	LOCATION OF VELOCITY PROFILE	LINEAR FIT	COEFFICIENT OF DETERMINATION (r^2)
h.d.	Dune trough	$y = -3.711 + 0.115x$	0.819
	Half-way up stoss side	$y = -109.262 + 1.016x$	0.744
	Dune crest	$y = -10.775 + 0.193x$	0.825
	Dune trough	$y = -5.134 + 0.172x$	0.826
		LOGARITHMIC FIT	COEFFICIENT OF DETERMINATION (r^2)
h.d.	Dune trough	$y = -21.908 + 6.694 \text{ Log}_e x$	0.715
	Half-way up stoss side	$y = -550.781 + 117.714 \text{ Log}_e x$	0.747
	Dune crest	$y = -59.477 + 15.072 \text{ Log}_e x$	0.736
	Dune trough	$y = -27.175 + 8.632 \text{ Log}_e x$	0.691
		EXPONENTIAL FIT	COEFFICIENT OF DETERMINATION (r^2)
h.d.	Dune trough	$y = 0.035 \exp(0.046x)$	0.996
	Half-way up stoss side	$y = 0.0001 \exp(0.823x)$	0.823
	Dune crest	$y = 0.009 \exp(0.058x)$	0.975
	Dune trough	$y = 0.047 \exp(0.051x)$	0.966
		POWER FIT	COEFFICIENT OF DETERMINATION (r^2)
h.d.	Dune trough	$y = 0.0001(x^{2.829})$	0.995
	Half-way up stoss side	$y = 0.0001(x^{34.319})$	0.837
	Dune crest	$y = 0.0001(x^{4.830})$	0.997
	Dune trough	$y = 0.0001(x^{2.855})$	0.996

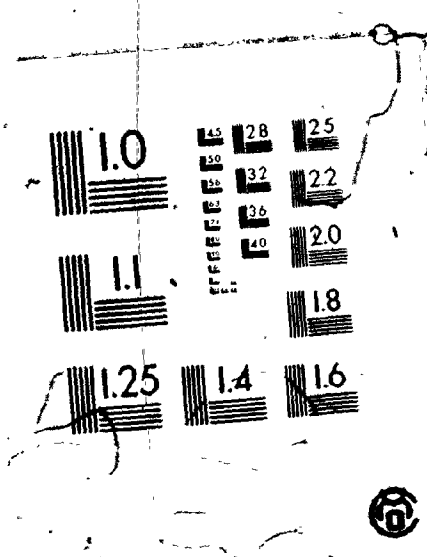

RUN #11

BED-FORM*	LOCATION OF VELOCITY PROFILE	LINEAR FIT	COEFFICIENT OF DETERMINATION (r^2)
h.d.	Dune trough	$y = -18.437 + 0.257x$	0.880
almost plane bed	Half-way up stoss side	$y = -25.584 + 0.337x$	0.886
	Dune crest	$y = -18.328 + 0.256x$	0.807
	Dune trough	$y = -9.667 + 0.181x$	0.800
		LOGARITHMIC FIT	**COEFFICIENT OF DETERMINATION (r^2)**
h.d.	Dune trough	$y = -107.481 + 25.123 \text{Log}_e x$	0.852
almost plane bed	Half-way up stoss side	$y = -147.07 + 33.946 \text{Log}_e x$	0.504
	Dune crest	$y = -96.553 + 22.793 \text{Log}_e x$	0.990
	Dune trough	$y = -52.488 + 13.379 \text{Log}_e x$	0.685
		EXPONENTIAL FIT	**COEFFICIENT OF DETERMINATION (r^2)**
h.d.	Dune trough	$y = 0.002 \exp(0.07x)$	0.861
almost plane bed	Half-way up stoss side	$y = 0.003 \exp(0.07x)$	0.504
	Dune crest	$y = 0.001 \exp(0.078x)$	0.990
	Dune trough	$y = 0.073 \exp(0.042x)$	0.886
		POWER FIT	**COEFFICIENT OF DETERMINATION (r^2)**
h.d.	Dune trough	$y = 0.0001(x^{7.167})$	0.914
almost plane bed	Half-way up stoss side	$y = 0.0001(x^{7.085})$	0.493
	Dune crest	$y = 0.0001(x^{7.287})$	0.999
	Dune trough	$y = 0.0001(x^{3.563})$	0.964

RUN #12

BED-FORM*	LOCATION OF VELOCITY PROFILE	LINEAR FIT	COEFFICIENT OF DETERMINATION (r^2)
plane bed	Profiles at 1 m.	$y = -23.216 + 0.156x$	0.806
	intervals along	$y = -22.358 + 0.149x$	0.790
	the bed.	$y = -24.394 + 0.154x$	0.818
		LOGARITHMIC FIT	**COEFFICIENT OF DETERMINATION (r^2)**
plane bed	Profiles at 1 m.	$y = -126.015 + 25.235 \text{ Log}_e x$	0.759
	intervals along	$y = -121.654 + 24.341 \text{ Log}_e x$	0.734
	the bed.	$y = -134.685 + 26.654 \text{ Log}_e x$	0.768
		EXPONENTIAL FIT	**COEFFICIENT OF DETERMINATION (r^2)**
plane bed	Profiles at 1 m.	$y = 0.0001 \exp(0.07x)$	0.987
	intervals along	$y = 0.0001 \exp(0.062x)$	0.990
	the bed.	$y = 0.0001 \exp(0.063x)$	0.983
		POWER FIT	**COEFFICIENT OF DETERMINATION (r^2)**
plane bed	Profiles at 1 m.	$y = 0.0001(x^{11.766})$	0.996
	intervals along	$y = 0.0001(x^{10.508})$	0.998
	the bed.	$y = 0.0001(x^{11.228})$	0.995